Contrib Mineral Petrol (2004) 146: 463–484
DOI 10.1007/s00410-003-0509-3

ORIGINAL PAPER

Didier Laporte · Michael J. Toplis · Monique Seyler
Jean-Luc Devidal

A new experimental technique for extracting liquids from peridotite at very low degrees of melting: application to partial melting of depleted peridotite

Received: 2 January 2003 / Accepted: 23 July 2003 / Published online: 26 September 2003

Abstract A new technique that allows extraction of liquids from peridotite at degrees of melting ϕ as low as 0.2 wt% is presented. Microfractures that formed in the graphite sample container at the beginning of the experiments were used as traps for the liquid phase. Glass-filled cracks (or 'microdikes') unaffected by quench crystallisation were produced in all experiments and were analysed using standard electron microprobe techniques. Reversal experiments demonstrated that, at moderate degrees of melting (4.4 and 6.5 wt%), the segregated liquid was in equilibrium with the neighbouring peridotite. At very low degrees of melting (0.3 wt%), the liquid in the microdikes failed to fully equilibrate with the peridotite after 5 days and the sandwich technique was used in combination with the microdike technique to approach more closely the equilibrium composition of near-solidus partial melts. The microdike technique was used to study melting of a depleted peridotite at 1 GPa and 1,220 to 1,360 °C.

Introduction

The compositions of mid-ocean ridge basalts (MORB) and abyssal peridotites have both been used to argue that the process of partial melting of the mantle beneath oceanic spreading centres is closer to fractional melting than to batch melting (e.g. Johnson et al. 1990; Langmuir et al. 1992). Within this framework, it is clear that even when the total degree of melting is large, modelling the process of MORB generation requires knowledge of the compositions of liquids resulting from small degree melting of a range of increasingly depleted peridotite compositions. Another motivation for the study of very low degrees of melting of peridotites is to understand the origin of glass inclusions within mantle minerals, particularly those with SiO_2 concentrations in excess of 60%, $Na_2O + K_2O$ up to 11% and nepheline-normative compositions (Schiano et al. 1998; Draper and Green 1999): these inclusions have been interpreted as trapped liquids formed at degrees of melting $< 1\%$, but such extreme compositions have not yet been reproduced in partial melting experiments.

Experimental determination of liquid composition at low melt fraction is compromised by the substantial compositional modifications that occur upon quenching at the end of piston-cylinder experiments (e.g. Cawthorn et al. 1973; Takahashi and Kushiro 1983). An original solution to this problem was proposed by Johnson and Kushiro (1992), Hirose and Kushiro (1993), and Baker and Stolper (1994) who showed that partial melt could be extracted into a diamond aggregate placed next to the peridotite powder. In this way, the liquid trapped in the diamond aggregate is not in direct contact with the grains of the peridotite and, therefore, is not affected by quench modification at the end of the experiment. Using this technique, Baker and Stolper (1994) and Baker et al. (1995) made the first detailed study of the evolution of liquid compositions as a function of melt fraction ϕ (2–27%) in a fertile mantle composition at 1 GPa.

In this paper, we present a new experimental technique to separate and analyse small volumes of liquid from partially molten peridotites. In our experiments, the basaltic liquid is directly injected into cracks in the graphite container. This technique is perfectly suited to

Editorial responsibility: T.L. Grove

D. Laporte (✉) · J.-L. Devidal
Laboratoire Magmas et Volcans,
CNRS et Université Blaise Pascal,
OPGC, 5 rue Kessler,
63038 Clermont-Ferrand, France
E-mail: laporte@opgc.univ-bpclermont.fr
Tel.: +33-4-73346733
Fax: +33-4-73346744

M. J. Toplis
CRPG-CNRS, BP20, 54501 Vandoeuvre-lès-Nancy, France

M. Seyler
Laboratoire de Géosciences Marines, CNRS-UMR 7097,
Institut de Physique du Globe de Paris, Case 89,
4 place Jussieu, 75252 Paris cedex 05, France

the study of extremely low degrees of melting (down to 0.2%) because the volume of segregated liquid is very small: typically 0.01-0.001 mm^3 compared with a peridotite volume of $\approx$12 mm^3. This new technique was used to characterise the compositions of partial melts formed in a depleted mantle composition, Depma, at 1 GPa and temperatures from 1,220 to 1,360 °C. The bulk composition studied here is significantly more refractory, both in terms of mineralogy (low proportion of Cpx) and composition (e.g. high MgO, low Na_2O, Al_2O_3) than compositions used in previous studies (Baker and Stolper 1994; Robinson et al. 1998; Pickering-Witter and Johnston 2000; Schwab and Johnston 2001; Wasylenki et al. 2003). A detailed discussion of the effect of bulk composition on the nature of low-degree partial melts will be presented in a subsequent contribution, which considers melting of our composition at 1 and 0.5 GPa.

In light of the controversy that has surrounded extraction techniques in the past (e.g. Falloon et al. 1999), the principal aim of the present contribution is to assess the equilibrium nature of the liquid compositions produced in direct partial melting experiments. Not only have time series experiments been performed to constrain the timing of microdike formation and the run-duration required to reach equilibrium, but sandwich experiments have been performed to reverse the liquid compositions. Furthermore, in the course of this study, it became apparent that small but variable amounts of water are present in our experimental liquids and a separate series of experiments to quantify the effect of small amounts of water was also performed.

Experimental and analytical techniques

Partial melting experiments

Starting materials

Depleted mantle composition Depma is mineralogically and chemically a close match to abyssal peridotite KN3, a clinopyroxene- and spinel-bearing harzburgite from ultramafic outcrops located south of the Kane Fracture Zone, near its intersection with the Mid-Atlantic Ridge (Auzende et al. 1993). The compositions of the minerals suggest that they are the residue of approximately 15% melting of fertile mantle, close to clinopyroxene exhaustion (Ghose et al. 1996). Depma was prepared by mixing orthopyroxene (Opx), clinopyroxene (Cpx) and spinel (Sp) separated from KN3, and olivines (Ol) from San Carlos and Burma (mineral compositions are given in Table 1). The proportions of San Carlos Ol and Burma Ol were chosen to produce a mean composition equal to KN3 Ol (mg# = 90.9). The mineral separates from KN3 were cleaned in warm hydrochloric acid, rinsed in deionized water and hand-picked to remove grains carrying alteration products. The minerals were mixed in weight proportions equal to those estimated for peridotite KN3 (Seyler, unpublished data): 76.4% Ol, 18.2% Opx, 3.5% Cpx and 1.9% Sp (phase proportions and oxide concentrations are given in wt%, unless specified otherwise; Table 1). The mixture was first homogenised by grinding under ethanol in an agate mortar. Because a fine grain size is critical to the attainment of chemical equilibrium, the mixture was then loaded in a micronising mill along with 12 ml ethanol and pulverised for 30 min: the typical grain size at the end of this treatment is 2–4 μm and the bigger grains are only 10 μm long and 5 μm wide (and only a few micrometres thick). The starting material was fired for 3 h at 900 °C in a CO_2/H_2 atmosphere with gas flow rates adjusted to yield an oxygen fugacity between the magnetite–wüstite and the iron–wüstite buffers ($f_{O2} = 10^{-15.91}$ bar). Powder Depma was stored under vacuum to minimise the adsorption of water.

Table 1 Composition of starting materials (wt%). The compositions of peridotite Depma and gels B2, B6 and B8 were analysed by ICP-AES at the Service d'Analyses des Roches et Minéraux (CRPG, Nancy); K_2O in Depma was analysed by atomic absorption spectroscopy (relative error: ±20%)

	Ol[a]			Opx[b]	Cpx[b]	Sp[b]	Depma[c]	Synthetic basalts[d]			
	Burma	SCO	Mean					B2	B6	B8	B2*
Na_2O	-	-	-	-	0.09	-	0.021	1.50	0.28	0.43	1.68
MgO	49.97	48.42	49.71	32.59	16.89	17.82	44.43	9.75	16.12	13.55	9.70
K_2O	-	-	-	-	-	-	0.005	2.14	-	0.07	2.21
CaO	0.03	0.08	0.04	1.27	22.37	-	1.20	12.09	11.51	13.82	11.20
TiO_2	-	-	-	0.04	0.10	0.06	0.02	0.50	0.23	0.31	0.54
FeO_{tot}	8.54	10.24	8.83	6.11	2.78	12.73	8.10	5.94	7.95	7.07	5.99
MnO	0.13	0.14	0.13	0.15	0.10	0.17	0.13	0.12	0.15	0.12	0.15
Cr_2O_3	-	-	-	0.84	1.17	25.47	0.68	0.04	0.38	0.28	0.10
SiO_2	41.30	41.10	41.27	54.80	51.63	0.02	43.56	49.27	48.83	48.57	50.36
Al_2O_3	0.02	0.02	0.02	4.18	4.86	43.67	1.86	18.63	14.56	15.77	18.07
Total[e]	99.10	98.96	99.67	99.91	99.20	98.31	99.04	99.14	99.43	99.39	100.00
mg#[f]	91.25	89.39	90.94	90.48	91.54	71.39	90.72	74.55	78.34	77.36	74.27

[a]The compositions of gem crystals of Ol from Burma and San Carlos (SCO) were analysed with an electron microprobe. The weighted mean composition of Ol in mineral powder Depma is given in column no. 4

[b]Opx, Cpx and Sp were separated from abyssal peridotite KN3 and analysed with an electron microprobe

[c]Depleted mantle composition Depma was prepared by mixing Ol, Opx, Cpx and Sp in the weight proportions of 76.4/18.2/3.5/1.9

[d]Compositions of the synthetic basalts used in the sandwich experiments (see text for more information)

[e]Original analytical totals (all compositions in the table have been recalculated to 100%)

[f]$mg\# = Mg^{2+}/(Mg^{2+} + Fe^{2+})$, where Mg^{2+} and Fe^{2+} are cation fractions and all iron is as Fe^{2+}

Table 2 Temperature, duration and modes in partial melting experiments of composition Depma at 1 GPa

Run no.	T	t	Phase assemblage and mode (wt%)[a]				
	(°C)	(h)	Ol	Opx	Cpx	Sp	Liquid
#21[b]	1,220	96.0	76.6 (41)	16.7 (47)	5.4 (15)	1.4 (5)	0.18 (8)
#2[b]	1,240	116.4	72.6 (39)	20.9 (48)	4.9 (15)	1.3 (4)	0.30 (12)
#18[b]	1,255	88.5	74.9 (34)	19.0 (43)	3.7 (16)	1.3 (4)	0.97 (25)
#3[c]	1,270	89.7	Ol + Opx + Cpx + Sp + liquid				
#5	1,285	79.5	74.1 (23)	20.6 (31)	1.3 (15)	1.1 (3)	2.5 (4)
#11	1,290	68.0	72.6 (27)	22.2 (38)	1.1 (18)	1.1 (3)	2.3 (5)
#8	1,300	70.0	74.8 (20)	19.7 (24)	Absent	0.8 (2)	4.4 (5)
#17	1,330	62.3	74.2 (29)	18.8 (35)	Absent	0.6 (3)	5.4 (9)
#6	1,360	56.0	73.9 (18)	18.6 (23)	Absent	0.5 (2)	6.5 (7)
#19[d]	1,300	1.0	Ol + Opx + Sp + liquid				
#20[d]	1,300	12.0	Ol + Opx + Sp + liquid				
#22[d]	1,300	24.2	Ol + Opx + Sp + liquid				

[a]The proportions of liquid and solid phases best fitting bulk composition Depma were calculated using a mass balance program modified from Albarède and Provost (1977; A. Provost, oral communication 2002). The errors (in parentheses) are given in terms of the least unit cited: e.g. 76.6 (41) and 0.18 (8) represent 76.6 ± 4.1 and 0.18 ± 0.08, respectively

[b]Well-developed basaltic microdikes were observed in runs #2 and #18 although no interstitial liquid was visible within the peridotite in back-scattered electron micrographs. In run #21, glass was only found within very thin veinlets ($<$ 1 μm thick) in the graphite lid

[c]The liquid phase in sample #3 could not be analysed because the graphite container was destroyed during sample preparation

[d]Three shorter duration experiments at 1,300 °C were performed to study the evolution of the basaltic microdikes with time. Only liquid and olivine (+ spinel in run #20) were analysed in these experiments so it was not possible to compute the modes

Experimental techniques

In the partial melting experiments, depleted peridotite Depma was subjected to a pressure of 1 GPa and a temperature, T, in the range 1,220–1,360 °C for durations of 56–116 h (Table 2). All the experiments were run in a non end-loaded, 3/4-inch piston-cylinder apparatus. From the outside to the inside, assemblies consist of a NaCl cell wrapped in lead foil, an outer Pyrex cylinder, a graphite furnace, an inner Pyrex cylinder and inner pieces of crushable MgO. Before each experiment, the assembly was dried for at least 24 h at 150 °C. Piston-cylinder assemblies using a NaCl cell require little or no friction correction (Boettcher et al. 1981). Calibration runs on the melting curve of NaCl showed that the frictional pressure loss was $\leq$ 50 MPa at 1 GPa and ≈1,000 °C; in this study, the frictional pressure loss is almost certainly lower than this value due to the higher run T. Temperature was controlled to within ≈1 °C of the set-point using calibrated W95Re5/W74Re26 thermocouples. Power output was monitored to ensure that no long-term temperature drift occurred during the runs. The experiments were terminated by shutting off the power to the apparatus; the quench rate was ≈50 °C/s.

We used double containers made of a graphite crucible fitted into a platinum capsule (outer diameter: 5 mm; wall thickness: 0.2 mm; Fig. 1). The graphite container was loaded with 20–25 mg of powder Depma, and then put into the platinum capsule and covered with a graphite lid. The platinum capsule was dried in an oven at 150 °C for at least 2 h and then rapidly welded shut while still hot. To ensure good temperature reproducibility, the sample was placed at exactly the same height (to within 0.1 mm) in the graphite furnace in all experiments: the bottom of the sample chamber was located at the hot spot of the furnace and the temperature at the top of the sample chamber was close to the temperature at the thermocouple tip (Fig. 1). The thermocouple tip was separated from the platinum capsule by a hard alumina disc, only 0.5 mm thick.

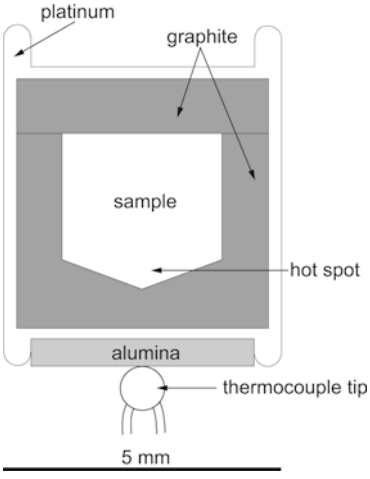

Fig. 1 Container geometry

Reversal experiments

We performed three series of experiments to reverse the results of partial melting experiments #6 at 1,360 °C, #8 at 1,300 °C and #2 at 1,240 °C: the aim was to verify that the glass compositions analysed in these experiments were at or close to equilibrium. For the reversal experiments, we used the 'sandwich' technique where a layer of basalt is forced to equilibrate with the peridotite powder at a pressure and temperature equal to those of the direct partial melting experiment (e.g. Falloon et al. 1999). If the composition of the starting basalt is at equilibrium with the peridotite, then, after equilibration, the basalt should form a liquid with unchanged composition, and the solid peridotite phases in contact with the melt at the end of the experiment should also be identical to those in the partial melting experiment.

In most sandwich experiments (rev2a–c, rev6a–b and rev8a–c; Table 3), the sandwiches were prepared by packing a thin layer of basalt (5–9 mg) on top of peridotite powder Depma in the graphite container. In the last experiments (rev2d–g and rev8d), the lower layer was a mixture of Depma and basalt to favour chemical interactions between basalt and peridotite by increasing the fraction of interstitial liquid in the peridotite. The total mass fraction of basalt in the sandwich experiments ranged from 21 to 55% (Table 3).

Six synthetic basalts were used in reversal experiments: three nominally anhydrous basalts (B2, B6 and B8) and three hydrous

Table 3 Reversal experiments: a summary of run information[a]

Run no.	wt% H_2O[b]	T (°C)	t (h)	wt% basalt[c]	β layer[d] (μm)	Cpx crust[e] (μm)	Peridotite paragenesis[f]
rev2a	NAB	1,270	83.1	34.8 (0)	650	50–100	Ol + Opx + Cpx + Sp + liquid
rev2b	NAB	1,280	73.5	≈26 (0)	300	0–50	Ol + Opx + Cpx + Sp + liquid
rev2c	NAB	1,295	80.5	20.9 (0)	250	≈0	Ol + Opx + Sp + liquid
rev2d	NAB	1,255	96.0	29.4 (15.6)	75	150	Ol + Opx + Cpx + Sp + liquid
rev2e	NAB	1,270	93.2	28.5 (15.6)	100	100	Ol + Opx + Cpx + Sp + liquid
rev2f	0.9 (0.60)	1,240	85.9	49.0 (33.6)	200	170	Ol + Opx + Cpx + Sp + liquid
rev2g	1.8 (1.13)	1,240	83.4	55.1 (32.9)	650	70	Ol + Opx + Sp + liquid
rev6a	NAB	1,375	57.9	23.9 (0)	Pools	Absent	Ol + Opx + Sp + liquid
rev6b	NAB	1,360	59.0	27.1 (0)	Pools	Absent	Ol + Opx + Sp + liquid
rev8a	NAB	1,300	70.2	35.1 (0)	Pools	130	Ol + Opx + Sp + liquid
rev8b	NAB (0.28)	1,315	59.9	31.9 (0)	Pools	100	Ol + Opx + Sp + liquid
rev8c	NAB	1,330	62.2	29.7 (0)	Pools	Absent	Ol + Opx + Sp + liquid
rev8d	0.5 (0.50)	1,300	67.1	50.7 (33.4)	Pools	60	Ol + Opx + Sp + liquid

[a]All the reversal experiments were made at 1 GPa in a piston-cylinder apparatus. The synthetic basalts used for the reversal experiments were B2 for runs rev2a–e, B2* for runs rev2f–g, B6 for runs rev6a–b and B8 for runs rev8a–d

[b]Water contents in the basalt. In most experiments, the starting basalt was nominally anhydrous ('NAB'). In three experiments, the starting basalt contained some dissolved water: 0.9wt% in rev2f, 1.8 wt% in rev2g and 0.5 wt% in rev8d. The numbers in parentheses are the water contents measured by ion microprobe in the basaltic glasses at the end of the experiments: 0.60 ± 0.12 in rev2f (three analytical spots); 1.13 ± 0.02 in rev2g (three spots); 0.50 ± 0.10 in rev8d (two spots); and 0.28 ± 0.02 (three spots) in the nominally anhydrous experiment rev8b. Water contents were measured using the IMS 1270 ion microprobe of CRPG-CNRS, Nancy; see Deloule et al. (1995) and Deloule (2002) for details on the analytical technique and conditions

[c]Starting compositions: the first number is the total mass fraction of basalt in the graphite container; the number in parentheses is the mass fraction of basalt in the peridotite layer

[d]Thickness of the layer of basaltic glass at the end of the experiment (in series rev2). In series rev6 and rev8, the basaltic glass was not present as a distinct layer, but formed two large, three-sided pools at the upper corners of the sample chamber (in three-dimensions, these pools correspond to a glass ring)

[e]Thickness of the clinopyroxenite layer. In runs rev2d–f and rev8a, the clinopyroxenite is Sp-bearing

[f]Paragenesis in the peridotite layer

Table 4 Mean glass compositions (wt%) measured in the basaltic microdikes of the partial melting experiments[a]

Run no.	#21 (3)	#2 (4)	#18 (8)	#5 (9)	#11 (8)	#8 (7)	#17 (6)	#6 (9)	#19 (3)	#20 (3)	#22 (4)
T (°C)	1,220	1,240	1,255	1,285	1,290	1,300	1,330	1,360	1,300	1,300	1,300
Na_2O	2.10 (21)	1.61 (3)	1.30 (6)	0.79 (5)	0.84 (5)	0.43 (3)	0.36 (3)	0.28 (3)	0.41 (7)	0.36 (5)	0.47 (5)
MgO	7.94 (37)	9.80 (12)	11.24 (11)	12.33 (9)	12.98 (18)	13.76 (16)	14.19 (29)	15.81 (14)	13.38 (71)	13.30 (14)	13.25 (15)
K_2O	3.32 (23)	2.07 (11)	0.64 (2)	0.23 (4)	0.27 (5)	0.13 (3)	0.06 (2)	0.05 (3)	0.11 (3)	0.11 (4)	0.10 (1)
CaO	10.13 (17)	11.86 (21)	12.97 (9)	13.49 (17)	13.46 (15)	13.63 (9)	12.71 (15)	11.40 (16)	12.88 (9)	13.46 (14)	13.84 (13)
TiO_2	0.58 (2)	0.51 (8)	0.53 (3)	0.46 (5)	0.45 (5)	0.33 (4)	0.26 (7)	0.23 (6)	0.27 (4)	0.30 (9)	0.33 (4)
FeO_{tot}	5.41 (31)	6.02 (14)	6.82 (11)	7.09 (12)	6.96 (17)	7.44 (11)	7.79 (20)	8.21 (14)	6.93 (9)	7.02 (16)	7.14 (6)
MnO	0.07 (7)	0.15 (3)	0.14 (3)	0.15 (4)	0.14 (3)	0.12 (4)	0.14 (4)	0.16 (4)	0.20 (1)	0.14 (2)	0.10 (3)
Cr_2O_3	0.05 (4)	0.04 (3)	0.11 (3)	0.15 (6)	0.18 (4)	0.31 (4)	0.30 (5)	0.38 (5)	0.28 (3)	0.27 (1)	0.26 (4)
SiO_2	51.10 (33)	49.79 (9)	48.32 (18)	48.66 (21)	48.50 (22)	48.48 (17)	48.92 (27)	49.21 (8)	50.32 (28)	49.43 (24)	48.63 (17)
Al_2O_3	19.31 (6)	18.15 (10)	17.94 (15)	16.65 (23)	16.22 (20)	15.37 (10)	15.25 (17)	14.27 (19)	15.21 (40)	15.61 (13)	15.87 (13)
Sum[b]	72.71 (354)	98.11 (50)	98.85 (51)	97.72 (53)	98.52 (67)	98.39 (30)	98.54 (80)	99.07 (75)	98.34 (59)	97.14 (119)	98.45 (5)
$mg\#_{liq}$[c]	72.32 (201)	74.35 (34)	74.59 (37)	75.61 (36)	76.88 (49)	76.72 (35)	76.46 (51)	77.44 (36)	77.44 (115)	77.15 (53)	76.79 (9)
$mg\#_{Ol}$[d]	90.53 (23)	90.57 (10)	90.39 (16)	90.47 (10)	90.41 (7)	90.61 (9)	90.41 (7)	90.71 (6)	90.88 (3)	90.81 (16)	90.60 (9)
$cr\#_{Sp}$[d]	26.42 (245)	28.00 (119)	27.30 (80)	30.34 (227)	28.24 (150)	31.59 (247)	39.61 (59)	42.88 (87)	-	31.56	-
K_D[e]	0.274 (36)	0.302 (14)	0.312 (15)	0.327 (12)	0.353 (17)	0.341 (13)	0.345 (20)	0.351 (12)	0.345 (26)	0.342 (18)	0.343 (13)

[a]All compositions are normalised to a sum of 100 %. Glass compositions were determined by electron probe microanalysis (conditions: 15 kV, 8 nA, and counting times of 10 s). The numbers in parentheses after the mean values are 1σ standard deviations, given in terms of the least unit cited: e.g. 1.61 (3) and 28.00 (119) represent 1.61 ± 0.03 and 28.00 ± 1.19, respectively. The number of analyses per sample is given in parentheses after the run number. We used a probe size of 5 μm for all samples except #6, #17, #19, #20, #22 (beam size: 2 μm) and #21 (1- or 2-μm beam size)

[b]Original analytical totals (before normalisation to a sum of 100%). The low analytical total in #21 is due to beam overlap onto graphite (the thickness of the glass veins in run #21 is < 1 μm)

[c]$mg\#_{liq} = 100\ Mg^{2+}/(Mg^{2+} + Fe^{2+})$ in the liquid phase, where Mg^{2+} and Fe^{2+} are cation fractions and all iron is as Fe^{2+}

[d]Compositions of the solid phases of the partially molten peridotite are indicated by the Ol mg#($mg\#_{Ol}$) and by the Sp cr#: $cr\#_{Sp} = 100\ Cr^{3+}/(Cr^{3+} + Al^{3+})$, where Cr^{3+} and Al^{3+} are cation fractions

[e]K_D is the partition coefficient of iron and magnesium between olivine and liquid: $K_D = (Fe^{2+}/Mg^{2+})_{Ol}/(Fe^{2+}/Mg^{2+})_{liq}$, where all iron is as Fe^{2+}

basaltic compositions (B2*/0.9 with 0.9% H_2O, B2*/1.8 with 1.8% H_2O and B8/0.5 with 0.5% H_2O). Nominally anhydrous basalts were directly synthesised as gels; after firing (at the same T and f_{O2} as Depma), the basaltic gels were stored under vacuum. The compositions of basaltic gels B2, B6 and B8 (Table 1) are a good match with the glass compositions in partial melting experiments #2, #6 and #8, respectively (Table 4).

On a H_2O-free basis, hydrous basalt B8/05 has a composition similar to B8. Column B2* in Table 1 gives the composition of hydrous basalts B2*/0.9 and B2*/1.8 on a H_2O-free basis. Comparison with glass #2 shows that composition B2* has a lower CaO content (11.2 versus 11.9%) and a larger SiO_2 content (50.4 versus 49.7%); the reason for these differences will be explained below. To synthesise the hydrous basalts, we first prepared iron-free, hydrous glasses by hydrating a basaltic gel in a piston-cylinder apparatus at 1,400 °C, 1 GPa for 4 h: 30–55 mg of a gel having a composition equivalent to B2* or B8 (but with no iron) were loaded in a platinum capsule along with a precisely weighed mass of tri-distilled water. The amount of water dissolved in the basaltic glass (3–5%) was computed from the masses of basaltic gel and water and was checked by loss on ignition at the end of the experiments. Basalts B2*/0.9, B2*/1.8 and B8/0.5 were obtained by mixing in the correct proportions the iron-free and H_2O-bearing glasses, the anhydrous basaltic gels and iron oxide (FeO).

Analytical techniques

At the end of an experiment, the whole platinum capsule was mounted in epoxy, sectioned lengthwise, polished and carbon-coated for scanning electron microscopy and electron probe microanalysis. Phase compositions were analysed with a Cameca SX-100 electron microprobe. For crystalline phases, a 15-kV accelerating voltage, a 15-nA beam current, counting times of 10 s, and a focussed beam were used. For glass analyses, the beam current was lowered to 8 nA and a beam size of 5 μm was used whenever possible, otherwise a beam diameter of 2 μm was used. Two sets of analyses of glass standard JDF–D2 (Reynolds and Langmuir 1997) were made using beam sizes of 2 and 5 μm. The average Na_2O contents were equal within error (2.89 ± 0.09% for a 2–μm beam size; 2.80 ± 0.07% for a 5–μm beam size) and compared well with the standard value (2.78 ± 0.05%). Accordingly, no correction for sodium loss was deemed necessary, even for glass analyses with a 2-μm beam size.

One microprobe session was devoted to more precise determinations of K_2O and to the measurement of Cl and P_2O_5 in glasses. We used procedures close to those described by Michael and Schilling (1989) and Reynolds and Langmuir (1997). Scapolite, orthoclase and apatite were used as standards for Cl, K_2O and P_2O_5, respectively. The accelerating voltage was 10 kV, the beam current was 100 nA and the counting times on peak positions were 20 s (+10 s on each of two symmetrically offset background positions). Tests were performed to check that the mean K_2O concentration was independent of beam size (between 5 and 20 μm). With the above procedure, we obtained K_2O concentrations in very good agreement with the concentrations obtained using our standard analytical procedure, but the standard deviation was reduced by one order of magnitude.

Results

Partial melting experiments

Textures, phase equilibria and modes

Textures of the partially molten peridotites are shown in Fig. 2a–c and the modal fractions of solid phases and

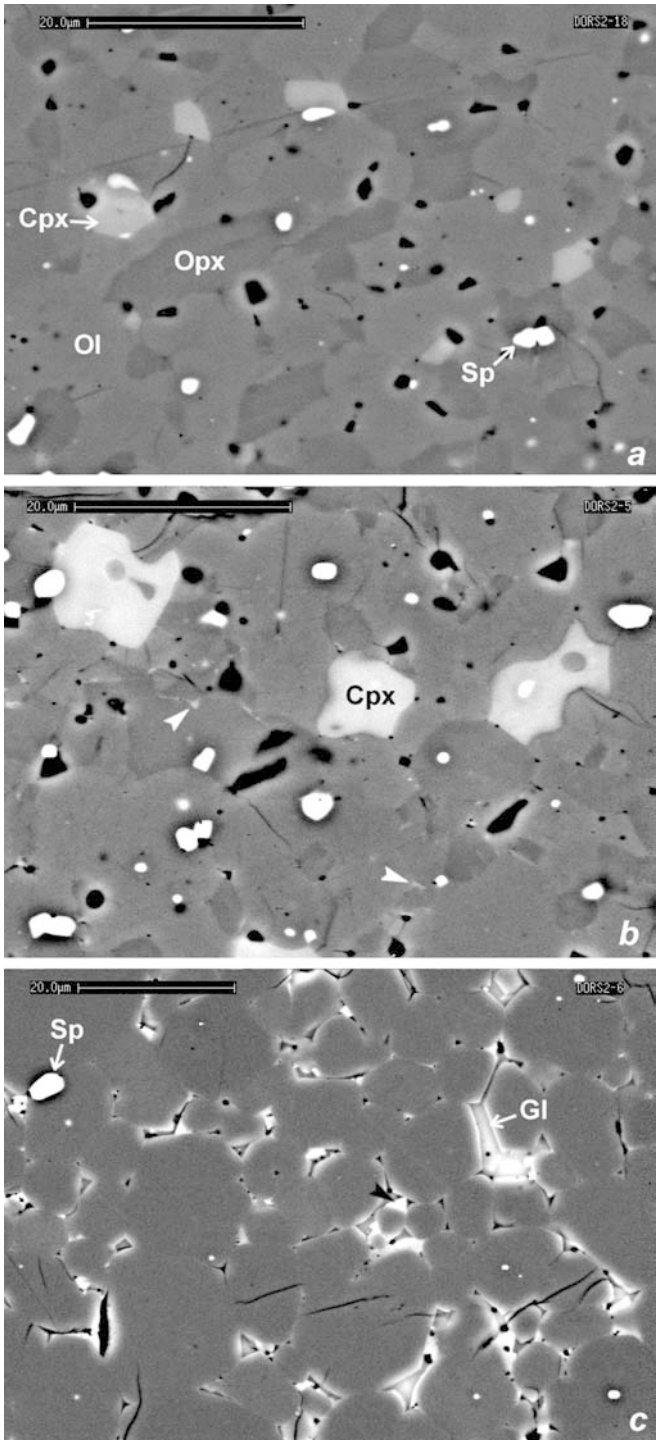

Fig. 2a–c Backscattered electron micrographs of polished sections illustrating the textures and parageneses in the partial melting experiments; *Ol* is grey, *Opx* is slightly darker than Ol, *Cpx* is light grey and *Sp* is white. **a** At 1,255 °C (run #18), Ol, Opx, Cpx and Sp form a near-equilibrium texture; interstitial glass is not visible due to its low fraction: ≈1.0%. **b** Sample #5 (1,285 °C) shows small glass pockets (*white arrows*) in addition to the four-phase assemblage Ol + Opx + Cpx + Sp; melt fraction in this sample is ≈2.5%. **c** In sample #6 (1,360 °C), the paragenesis is Ol + Opx + Sp + liquid and the melt fraction is ≈6.5% (*Gl*: glass); Cpx occurs as quench overgrowths (*black arrow*) around Opx. *Scale bars* are 20 μm

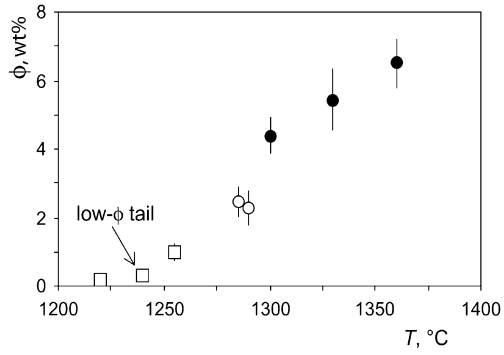

Fig. 3 Plot of melt fraction ϕ (wt%; from Table 2) as a function of run temperature, T. *Solid circles*: liquid in equilibrium with Ol + Opx + Sp; *empty symbols* liquid in equilibrium with Ol + Opx + Cpx + Sp. The 'low-ϕ tail' (*empty squares*) correspond to a group of experiments in which glass-filled cracks were observed in the graphite container, but no interstitial liquid was detected in backscattered electron micrographs (as in Fig. 2a). Partial melting at temperatures ≤ 1,270 °C is due to the presence of trace amounts of water in the experiments

liquid in the run products are summarised in Table 2. Significant grain growth occurred in all the experiments and resulted in near-equilibrium textures with grain sizes about five times larger than the grain size of the starting material (2–4 μm). At high T (1,360 °C; Fig. 2c) Ol grains exceeded 20 μm and Opx grains reached 10–15 μm in diameter. At lower T, grain growth was not so prominent, but a high degree of textural equilibration was still attained owing to the very small grain size of our starting material. For instance, the microtexture of sample #18 (1,255 °C; Fig. 2a) is characterised by polygonal grain shapes with plane or slightly curved grain boundaries and grain-boundary angles close to 120° as expected in a well-annealed polycrystal (Smith 1964).

In terms of phase stability, two fields may be distinguished as a function of temperature:

1. For T ≤ 1,290 °C, Cpx is present in addition to Ol, Opx, Sp and liquid (Fig. 2a, b). It occurs as relatively large grains in which most of the grain boundaries are slightly concave. Cpx abundance decreases from ≈5% at 1,220 °C to ≈1% at 1,290 °C. In samples #5 ►

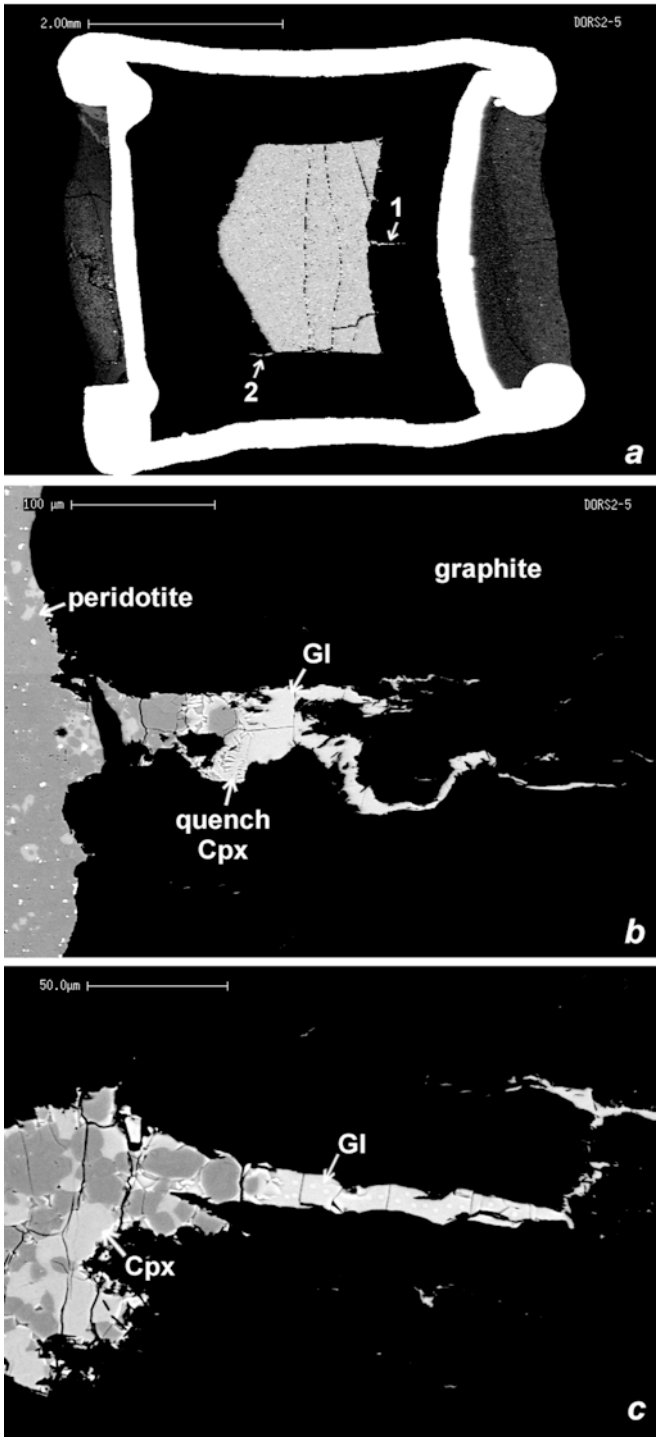

Fig. 4a–c Backscattered electron micrographs of the basaltic microdikes in the partial melting experiments (the three micrographs are rotated 90° clockwise compared with Fig. 1: top is on the right). **a** A lengthwise section of sample #5 showing the platinum container (*white*), the graphite container (*black*), the partially molten peridotite (*grey*) and two dikes rooted in the peridotite and cutting the inner part of the graphite container: dike no. 1, in the *central part of the graphite lid*, is a basaltic microdike with a glass-filled tip; dike no. 2, at the *lower edge of the graphite container*, is filled with peridotite minerals. **b** Basaltic microdike in run #5: the lower part of the dike (*on the left*) is filled with crystals; the upper part is filled with segregated glass. Quench Cpx grew as dendrites at the base of the glass pool. **c** Well-developed basaltic microdike in a low-T partial melting experiment (#18, 1,255 °C); the *white dots* in the glass are electron microprobe spots. *Scale bars*: 2 mm in **a**, 100 μm in **b** and 50 μm in **c**

(1,285 °C) and #11 (1,290 °C), melt fraction is equal to 2–2.5% (Table 2) and the interstitial liquid is easily visible in the peridotite, mostly as irregular three-sided pockets (Fig. 2b). At T ≤ 1,270 °C, no interstitial liquid was detected in backscattered electron micrographs (Fig. 2a), but glass-filled cracks were observed in the graphite container, and secondary electron imaging of fracture surfaces of the peridotite revealed the presence of some melt at grain corners and along grain edges. In addition, melt fractions of

0.2% at 1,220 °C to 1% at 1,255 °C were calculated by mass balance (Fig. 3). As argued in the Discussion section, we believe that the anhydrous solidus temperature of Depma at 1 GPa is 1,270–1,280 °C, the presence of partial melt at temperatures as low as 1,220 °C being due to the presence of trace amounts of water in the experiments.

2. For T ≥ 1,300 °C, Cpx is only present as quench overgrowths around Opx and the equilibrium phase assemblage is Ol + Opx + Sp + liquid. Melt fraction increases with increasing T: but, even at 1,360 °C, it remains small (6.5%; Fig. 2c) because of the highly depleted nature of Depma.

The basaltic microdikes

In all the partial melting experiments, we observed a small number of dikes rooted in the peridotite and cutting the inner part of the graphite container over a length of up to 400 μm. In lengthwise sections of the samples, the dikes are located either at the edges of the sample chamber or in the central part of the graphite lid (Fig. 4a). Dikes at the edges of the sample chamber were not studied because they never contain pools of segregated liquid. On the contrary, the tip of the dikes in the central part of the graphite lid is filled with glass. These glass-filled cracks, hereafter referred to as basaltic microdikes, comprise three parts (Fig. 4b, c): (1) a lower part, typically 100 to 200 μm long, filled with impinging crystals of Ol, Opx, Cpx (only at T < 1,300 °C) and Sp with little interstitial liquid (the volume fraction of Cpx in the microdikes is larger than in the main body of peridotite; compare Figs. 2a and 4c); (2) a thin layer of Cpx dendrites formed during quench; and (3) an upper part consisting of a long vein of glass, free of crystals (except for graphite platelets).

Basaltic microdikes are typically 10 to 20 μm thick, but can be up to 50 μm thick (in run #5) or be only 5 μm thick (in run #17). Dike lengths range from 300 to 400 μm. These lengths are small compared with the thickness of the graphite lid (800–900 μm): in no case did the basaltic liquid reach the platinum container. In general no clear positive correlation between the size of the microdikes and the degree of melting in the peridotite is apparent. In particular, well-developed basaltic microdikes were observed even in experiments #2 (at 1,240 °C) and #18 (at 1,255 °C; Fig. 4c) although no interstitial liquid was observed within the peridotite in backscattered electron micrographs (Fig. 2a). A few glass-filled veins were also observed in run #21 (at 1,220 °C), but, in this case, they are much shorter (≈50 μm) and thinner (< 1 μm) than in the experiments at higher T.

From the overall shape of the graphite containers at the end of the experiments (Fig. 4a), we deduce that the formation of the basaltic microdikes resulted from downward bending of the graphite lid. As discussed below, time-series experiments at 1,300 °C showed that the fractures in the graphite lid formed early, presumably during the loading stage of the experiment, and were filled with liquid at the very beginning of the partial meting experiment.

Phase compositions

Liquid compositions In all the experiments except #21 at 1,220 °C, the basaltic microdikes were sufficiently wide

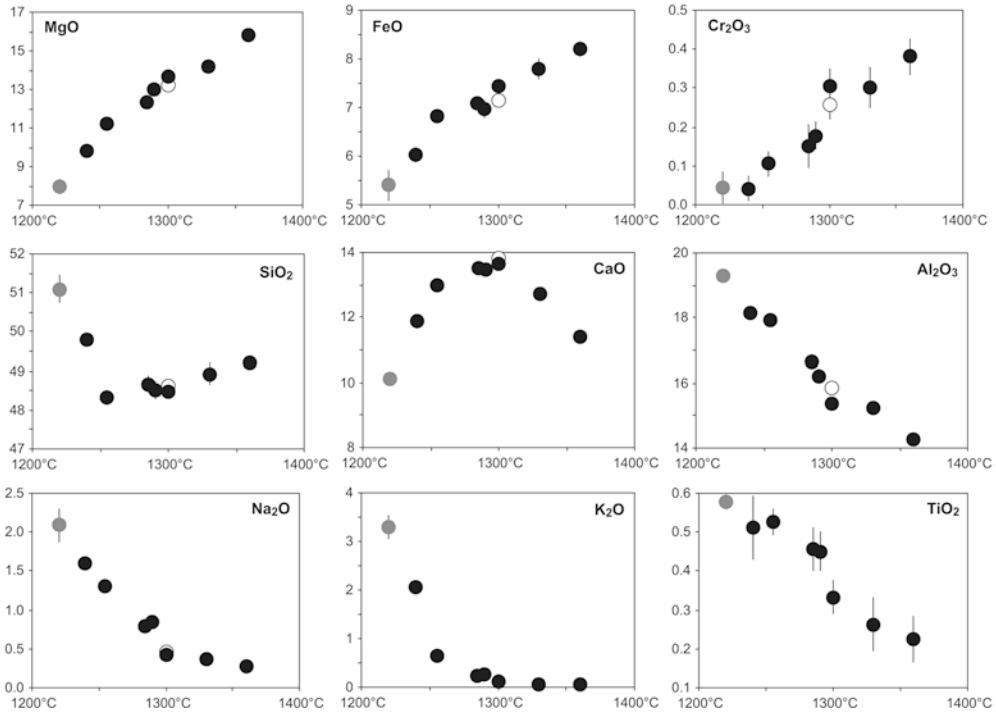

Fig. 5 Average oxide concentrations (wt%) in glass as a function of the temperature of the partial melting experiment (all compositions were normalised to a sum of 100% before plotting). When not visible, the error bar (1σ) is smaller than the *symbol*. The *grey circle* at 1,220 °C correspond to run #21 in which the average analytical total was only 72%. The *two circles* at 1,300 °C corresponds to two experiments of different durations: run #8, 70 h (*solid circle*) and run #22, 24.2 h (*empty circle*; not plotted in the K_2O and TiO_2 diagrams because indistinguishable from the solid circle)

Table 5 Average compositions of glass and solid phases in partial melting experiment #6 (1,360 °C, 1 GPa) and in reversal experiments rev6a (1,375 °C) and rev6b (1,360 °C)[a]

	Phase	Na_2O	MgO	K_2O	CaO	TiO_2	FeO	MnO	Cr_2O_3	SiO_2	Al_2O_3	Total	mg#	cr#
#6	Liquid (9)	0.28 (3)	15.81 (14)	0.05 (3)	11.40 (16)	0.23 (6)	8.21 (14)	0.16 (4)	0.38 (5)	49.21 (8)	14.27 (19)	99.07 (75)	77.44 (36)	
	Ol (6)		49.45 (12)		0.24 (2)		9.02 (5)	0.11 (5)	0.28 (5)	40.80 (10)	0.10 (1)	99.85 (34)	90.71 (6)	
	Opx (12)		32.52 (19)		1.53 (10)		5.49 (6)	0.13 (2)	1.32 (14)	55.02 (30)	3.99 (32)	99.29 (25)	91.35 (8)	
	Sp (6)		18.98 (30)				9.92 (7)	0.17 (2)	37.27 (72)	0.35 (11)	33.31 (59)	97.19 (79)	77.33 (29)	42.88 (87)
rev6a	Liquid (10)	0.27 (3)	17.42 (21)	0.04 (2)	10.41 (19)	0.21 (3)	8.44 (11)	0.17 (4)	0.59 (6)	49.23 (38)	13.21 (12)	99.54 (51)	78.62 (22)	
	Ol (4)		50.00 (11)		0.26 (2)		8.52 (16)	0.15 (3)	0.40 (5)	40.56 (18)	0.11 (1)	100.68 (20)	91.28 (15)	
	Opx (4)		32.85 (16)		1.54 (6)		5.40 (7)	0.12 (2)	1.53 (10)	54.54 (19)	4.02 (16)	100.92 (41)	91.56 (9)	
	Sp (3)		18.61 (2)				9.63 (13)	0.17 (10)	40.21 (83)	0.18 (3)	31.21 (79)	98.41 (22)	77.51 (25)	46.37 (115)
rev6b	Liquid (10)	0.35 (3)	14.94 (19)	0.08 (3)	12.29 (17)	0.28 (6)	8.03 (16)	0.19 (6)	0.34 (5)	48.27 (33)	15.23 (17)	99.29 (55)	76.84 (36)	
	Ol (7)		49.48 (14)		0.34 (4)		9.16 (11)	0.14 (2)	0.24 (3)	40.53 (16)	0.11 (2)	100.18 (43)	90.59 (11)	
	Opx (7)		32.48 (28)		1.79 (4)		5.50 (8)	0.13 (2)	1.38 (7)	54.35 (12)	4.38 (28)	100.19 (57)	91.33 (14)	
	Sp (5)		18.79 (18)				9.78 (10)	0.15 (2)	34.42 (47)	0.19 (2)	36.66 (29)	98.64 (21)	77.41 (21)	38.64 (51)

[a]Solid phase compositions were determined with an electron microprobe using a 15-kV accelerating voltage, a 15-nA beam current, counting times of 10 s and a focused beam. For glasses, we used a 8-nA beam current and a 5-μm beam size (2-μm in run #6). The numbers in parentheses after the mean values are 1σ standard deviations, given in terms of the least unit cited. The number of analyses per phase is given in parentheses in the second column. Original analytical totals are given in the column 'Total' (all compositions in the table are normalised to a sum of 100%)

to be analysed with an electron beam diameter of 2 or 5 μm. Good analytical totals (98–99%; Table 4) were obtained for the glasses in these experiments. In run #21, glass veins were less than 1 μm thick and it was not possible to obtain analytical totals better than 77% even with a focussed electron beam due to beam overlap onto the graphite container. After normalisation to 100%, glass #21 plots well on the smooth trends defined by the other glass compositions as a function of temperature (Fig. 5).

Over the entire range of temperature, MgO, FeO and Cr_2O_3 increase with increasing T from 1,220 to 1,360 °C, MgO increases from 7.9 to 15.8%, FeO from 5.4 to 8.2%, and Cr_2O_3 increases up to ≈0.4%. The concentrations of Na_2O, Al_2O_3 and TiO_2 decrease continuously with increasing T from 2.1, 19.3 and 0.6%, respectively, at 1,220 °C, to 0.3, 14.3 and 0.2% at 1,360 °C, respectively. The concentration of CaO shows a concave-downward pattern with a maximum value of 13.6% at 1,300 °C, coincident with the experimental brackets of Cpx-out (1,290–1,300 °C). The plot of SiO_2 as a function of T shows a very interesting pattern: with increasing T, SiO_2 first decreases from ≈51% at 1,220 °C to 48.3% at 1,255 °C, and then increases slightly to 49.2% at 1,360 °C. A strong enrichment in K_2O is observed in the lowest temperature experiments: glasses from runs #2 at 1,240 °C and #21 at 1,220 °C contain 2.1 and 3.3% K_2O, respectively.

Compositions of the solid phases A complete account of the compositions of the solid phases will be given in a companion paper on the partial melting of Depma at 0.5 and 1.0 GPa. In this paper, we need only highlight the following observations:

1. Within a single experimental charge, mineral compositions show little variability (see the standard deviations of oxide concentrations in solid phases in partial melting experiments #2, #6 and #8; Tables 5, 6 and 7); thus, the problem of incomplete homogenisation of natural mineral grains previously described in the literature (Falloon et al. 1999) would appear to have been minimised through the use of an extremely fine-grained starting material.
2. Significant variations of the composition of all solid phases are observed with increasing T: for example, Ol mg#'s and Opx mg#'s increase from 90.4 to 90.7 and from 90.7 to 91.3, respectively, and Cr_2O_3 in Sp increases from 25% at 1,220–1,270 °C to 37% at 1,360 °C (accompanied by a decrease in the Al_2O_3 content from 45 to 33%).
3. Solid phases were systematically analysed in the upper part of the sample chamber, typically 100 to 200 μm below the graphite lid. For comparison, we also analysed the compositions of the grains located in the lower part of the basaltic microdikes. In most experiments, these grains have compositions indistinguishable from those measured in the peridotite (see, for example, the data for run #8 in Table 6). In

Table 6 Average compositions of glass and solid phases in partial melting experiment #8 (1,300 °C, 1 GPa) and in reversal experiments rev8a–d[a]

	Phase[b]	Na_2O	MgO	K_2O	CaO	TiO_2	FeO	MnO	Cr_2O_3	SiO_2	Al_2O_3	Total	mg#	cr#
#8	Liquid (7)	0.43 (3)	13.76 (16)	0.13 (3)	13.63 (9)	0.33 (4)	7.44 (11)	0.12 (4)	0.31 (4)	48.48 (17)	15.37 (10)	98.39 (30)	76.72 (35)	
	Ol (5)		49.39 (8)		0.27 (2)		9.12 (10)	0.10 (2)	0.21 (4)	40.84 (17)	0.07 (1)	100.40 (48)	90.61 (9)	
	Ol, dike (5)		49.27 (10)		0.30 (1)		8.88 (10)	0.11 (3)	0.21 (2)	41.14 (14)	0.09 (1)	99.10 (26)	90.81 (9)	
	Opx (12)		31.80 (11)		2.39 (5)		5.53 (6)	0.13 (3)	1.18 (5)	54.59 (17)	4.38 (14)	99.61 (45)	91.10 (9)	
	Opx, dike (4)		31.41 (26)		2.47 (9)		5.32 (7)	0.14 (3)	1.25 (4)	54.65 (35)	4.76 (16)	99.48 (50)	91.31 (16)	
	Sp (5)		19.75 (32)				9.41 (13)	0.13 (4)	28.66 (175)	0.34 (9)	41.70 (218)	97.76 (59)	78.92 (19)	31.59 (247)
rev8a	Liquid (6)	0.62 (3)	12.64 (15)	0.16 (3)	13.54 (9)	0.36 (6)	7.52 (10)	0.14 (5)	0.16 (7)	47.92 (16)	16.95 (14)	99.53 (23)	74.96 (32)	
	Ol (8)		49.06 (15)		0.31 (2)		9.72 (13)	0.13 (3)	0.16 (3)	40.52 (16)	0.11 (2)	100.52 (53)	90.00 (14)	
	Opx (11)		30.92 (40)		2.53 (15)		5.88 (8)	0.12 (3)	0.97 (8)	53.31 (27)	6.27 (49)	100.55 (28)	90.35 (21)	
	Cpx (11)	0.12 (3)	20.61 (70)		16.15 (98)	0.07 (3)	4.17 (23)	0.14 (3)	1.16 (9)	50.96 (41)	6.61 (39)	99.79 (66)	89.81 (29)	
	Sp (10)		21.12 (25)				8.74 (19)	0.11 (3)	18.75 (105)	0.17 (3)	51.10 (131)	99.53 (79)	81.15 (24)	19.77 (128)
rev8b	Liquid (9)	0.54 (3)	12.97 (16)	0.13 (3)	13.52 (17)	0.39 (6)	7.41 (11)	0.13 (3)	0.24 (4)	48.33 (20)	16.33 (8)	99.97 (32)	75.73 (45)	
	Ol (5)		49.07 (11)		0.36 (3)		9.28 (15)	0.13 (6)	0.21 (4)	40.85 (9)	0.10 (2)	100.51 (26)	90.41 (15)	
	Opx (7)		31.20 (27)		2.54 (11)		5.60 (11)	0.13 (4)	1.13 (8)	53.71 (41)	5.70 (41)	100.52 (41)	90.86 (21)	
	Cpx (6)	0.11 (1)	21.13 (70)		15.67 (72)	0.09 (4)	4.06 (14)	0.12 (2)	1.30 (8)	51.62 (41)	5.89 (45)	100.55 (39)	90.26 (19)	
	Sp (6)		20.30 (34)				8.73 (12)	0.11 (3)	22.96 (23)	0.19 (2)	47.70 (28)	99.50 (65)	80.56 (39)	24.41 (25)
rev8c[c]	Liquid (10)	0.46 (3)	14.13 (12)	0.12 (4)	13.11 (19)	0.34 (4)	7.52 (11)	0.15 (4)	0.39 (4)	48.79 (18)	14.98 (14)	99.23 (31)	77.00 (29)	
	Ol (6)		49.52 (14)		0.33 (4)		8.93 (10)	0.12 (2)	0.26 (2)	40.75 (17)	0.09 (2)	99.76 (22)	90.82 (10)	
	Opx (6)		31.59 (26)		2.47 (7)		5.40 (9)	0.10 (2)	1.37 (9)	54.45 (16)	4.61 (26)	100.63 (41)	91.24 (16)	
	Sp (7)		19.04 (15)				9.46 (12)	0.15 (3)	33.30 (28)	0.20 (3)	37.84 (25)	99.89 (4)	78.21 (27)	37.12 (33)
rev8d	Liquid (12)	0,50 (3)	12.91 (26)	0.14 (3)	13.73 (21)	0.37 (5)	7.42 (10)	0.15 (4)	0.19 (3)	48.41 (29)	16.19 (21)	97.62 (138)	75.62 (54)	
	Ol (5)		48.75 (1)		0.36 (3)		9.45 (10)	0.10 (4)	0.15 (2)	41.12 (8)	0.08 (2)	99.51 (42)	90.19 (9)	
	Opx (6)		31.09 (13)		2.51 (9)		5.72 (7)	0.12 (4)	1.23 (9)	54.18 (34)	5.14 (26)	99.94 (54)	90.64 (10)	
	Cpx (7)	0,10 (2)	20.61 (29)		16.54 (29)	0.09 (2)	3.94 (13)	0.11 (4)	1.43 (9)	51.90 (27)	5.28 (41)	98.87 (62)	90.31 (20)	
	Sp (6)		19.01 (18)				9.64 (19)	0.14 (3)	28.01 (72)	0.18 (2)	43.02 (75)	98.99 (44)	77.84 (47)	30.40 (91)

[a]See note a in Table 5 for analytical details. All the glasses were analysed with a 5-μm beam size
[b]In run #8, 'Ol, dike' and 'Opx, dike' refer to the compositions of Ol and Opx in the lower part of the basaltic microdike
[c]The ratio $Fe^{3+}/(Fe^{2+}+Fe^{3+})$ in glass rev8c is equal to 0.03, as determined with an electron microprobe using the technique of Fialin et al. (2001)

Table 7 Average compositions of glass and solid phases in partial melting experiment #2 (1,240 °C, 1 GPa) and in reversal experiments rev2a–g[a]

	Phase[b]	Na_2O	MgO	K_2O	CaO	TiO_2	FeO	MnO	Cr_2O_3	SiO_2	Al_2O_3	Total	mg#	cr#
#2[c]	Liquid (4)	1.61 (3)	9.80 (12)	2.07 (11)	11.86 (21)	0.51 (8)	6.02 (14)	0.15 (3)	0.04 (3)	49.79 (9)	18.15 (10)	98.11 (50)	74.35 (34)	
	Ol (6)		49.61 (17)		0.26 (4)		9.21 (9)	0.12 (3)	0.15 (3)	40.58 (13)	0.06 (4)	100.83 (32)	90.57 (10)	
	Ol, dike (3)		49.31 (5)		0.24 (4)		9.47 (13)	0.12 (5)	0.08 (5)	40.70 (16)	0.08(2)	99.75 (100)	90.28 (12)	
	Opx (10)		32.73 (40)		1.92 (18)		5.84 (9)	0.12 (3)	0.96 (6)	54.27 (46)	4.16 (16)	100.99 (27)	90.90 (13)	
	Cpx (3)	0.21 (2)	18.77 (5)		19.34 (28)	0.12 (1)	3.35 (14)	0.10 (2)	1.29 (19)	51.67 (51)	5.13 (42)	100.43 (45)	90.91 (35)	
	Sp (5)		20.42 (17)				9.69 (13)	0.13 (2)	25.47 (96)	0.35 (12)	43.95 (94)	98.78 (37)	78.97 (35)	28.00 (119)
	Sp, dike (1)		24.43				8.25	0.17	10.12	0.13	56.91	95.43	84.08	10.66
rev2a	Liquid (7)	1.64 (6)	9.75 (10)	2.31 (8)	10.83 (11)	0.57 (7)	6.02 (15)	0.12 (2)	0.09 (3)	50.47 (26)	18.19 (20)	99.27 (50)	74.28 (56)	
	Ol (9)		49.33 (16)		0.29 (3)		9.43 (11)	0.13 (2)	0.09 (4)	40.63 (23)	0.09 (1)	100.38 (52)	90.32 (11)	
	Opx (7)		31.54 (40)		2.36 (11)		5.83 (7)	0.13 (4)	0.95 (9)	54.36 (40)	4.83 (50)	100.50 (29)	90.61 (16)	
	Cpx (9)	0.26 (2)	20.49 (49)		16.13 (53)	0.17 (3)	4.04 (13)	0.12 (3)	1.03 (20)	51.75 (39)	6.01 (30)	100.42 (45)	90.04 (33)	
	Sp (6)		22.19 (16)				8.19 (13)	0.09 (6)	13.60 (54)	0.22 (7)	55.73 (81)	99.18 (56)	82.85 (17)	14.07 (65)
rev2b	Liquid (8)	1.59 (7)	10.04 (13)	2.18 (9)	11.19 (14)	0.55 (4)	5.91 (10)	0.11 (4)	0.09 (4)	50.51 (27)	17.83 (20)	99.23 (37)	75.18 (43)	
	Ol (8)		49.43 (22)		0.30 (2)		9.33 (13)	0.14 (3)	0.13 (3)	40.57 (17)	0.10 (3)	100.70 (50)	90.43 (14)	
	Opx (4)		31.90 (41)		2.22 (19)		5.68 (13)	0.13 (3)	0.88 (8)	54.34 (37)	4.86 (51)	100.92 (27)	90.92 (24)	
	Cpx (9)	0.25 (2)	20.46 (59)		16.44 (63)	0.17 (4)	3.97 (18)	0.14 (3)	1.13 (11)	51.49 (23)	5.94 (42)	100.69 (74)	90.19 (35)	
	Sp (4)		21.94 (6)				8.45 (7)	0.11 (3)	15.31 (121)	0.19 (4)	54.00 (116)	98.30 (13)	82.23 (12)	15.98 (134)
rev2c[d]	Liquid (4)	1.39 (3)	10.96 (11)	1.94 (4)	11.38 (3)	0.47 (0)	6.26 (17)	0.14 (2)	0.18 (7)	50.27 (14)	17.01 (13)	99.61 (35)	75.72 (40)	
	Ol (3)		49.61 (5)		0.34 (3)		8.84 (20)	0.13 (1)	0.22 (6)	40.79 (15)	0.07 (2)	100.73 (9)	90.91 (19)	
	Sp (1)		20.50				8.65	0.11	23.20	0.17	47.25	98.20	80.86	24.78
rev2d	Liquid (6)	1.81 (5)	9.32 (7)	2.60 (11)	10.42 (19)	0.54 (6)	5.85 (10)	0.13 (4)	0.06 (2)	51.05 (15)	18.22 (14)	98.31 (43)	73.95 (45)	
	Ol (5)		49.04 (12)		0.27 (4)		9.36 (19)	0.15 (2)	0.09 (1)	41.01 (18)	0.08 (2)	99.96 (25)	90.33 (19)	
	Opx (4)		31.13 (20)		2.11 (17)		5.82 (11)	0.13 (3)	0.65 (3)	53.67 (20)	6.49 (30)	99.99 (35)	90.51 (19)	
	Cpx (5)	0.30 (2)	18.91 (30)		17.65 (31)	0.24 (3)	3.65 (11)	0.13 (2)	0.65 (23)	51.18 (18)	7.30 (54)	99.49 (17)	90.23 (30)	
	Sp (3)		22.19 (24)				8.13 (2)	0.11 (5)	13.05 (68)	0.27 (8)	56.24 (64)	97.16 (24)	82.94 (17)	13.47 (73)
rev2e	Liquid (7)	1.68 (6)	9.57 (12)	2.40 (11)	10.62 (11)	0.51 (6)	5.82 (10)	0.06 (5)	0.10 (1)	51.06 (15)	18.17 (16)	97.53 (37)	74.55 (50)	
	Ol (5)		48.85 (19)		0.29 (4)		9.20 (8)	0.11 (3)	0.12 (3)	41.36 (15)	0.09 (2)	99.15 (27)	90.45 (10)	
	Opx (5)		30.93 (16)		2.29 (6)		5.65 (7)	0.12 (2)	0.81 (2)	53.98 (22)	6.21 (30)	99.60 (24)	90.70 (11)	
	Cpx (8)	0.28 (4)	19.64 (34)		16.58 (36)	0.21 (3)	3.78 (16)	0.14 (4)	0.93 (14)	51.56 (22)	6.90 (41)	98.92 (46)	90.27 (32)	
	Sp (3)		21.93 (12)				7.97 (8)	0.10 (3)	12.81 (20)	0.22 (1)	56.96 (16)	96.85 (55)	83.05 (20)	13.11 (21)
rev2f	Liquid (6)	2.09 (4)	8.38 (11)	2.68 (9)	10.07 (11)	0.59 (5)	5.67 (4)	0.11 (6)	0.04 (2)	50.96 (21)	19.41 (9)	98.07 (59)	72.49 (16)	
	Ol (5)		48.38 (16)		0.30 (2)		10.24 (11)	0.12 (3)	0.06 (3)	40.84 (16)	0.08 (1)	99.10 (28)	89.39 (10)	
	Opx (6)		30.69 (31)		2.09 (9)		6.31 (11)	0.14 (2)	0.75 (6)	53.80 (35)	6.21 (59)	99.54 (5)	89.65 (17)	
	Cpx (10)	0.32 (4)	18.42 (32)		18.09 (61)	0.25 (3)	3.94 (18)	0.12 (4)	0.78 (15)	51.18 (26)	6.89 (31)	99.28 (42)	89.28 (33)	
	Sp (7)		20.87 (30)				8.77 (21)	0.10 (3)	12.27 (160)	0.20 (7)	57.78 (163)	99.28 (66)	80.92 (54)	12.48 (173)
rev2g	Liquid (7)	1.75 (7)	9.39 (5)	2.25 (7)	10.57 (16)	0.58 (7)	5.96 (9)	0.16 (4)	0.08 (4)	51.22 (13)	18.05 (13)	97.62 (26)	73.75 (31)	
	Ol (6)		48.71 (12)		0.24 (3)		9.66 (10)	0.14 (4)	0.13 (3)	41.05 (18)	0.07 (1)	99.15 (21)	89.99 (9)	
	Opx (6)		31.49 (17)		1.98 (33)		5.92 (16)	0.14 (3)	1.03 (7)	54.81 (27)	4.63 (19)	99.02 (23)	90.46 (25)	
	Cpx (7)	0.30 (3)	18.94 (57)		18.21 (72)	0.18 (3)	3.64 (15)	0.11 (4)	1.32 (15)	51.73 (55)	5.56 (69)	99.29 (39)	90.26 (27)	
	Sp (4)		19.14 (17)				9.70 (21)	0.11 (4)	26.00 (59)	0.17 (1)	44.89 (63)	98.70 (47)	77.86 (49)	27.98 (73)

[a]See note a in Table 5 for analytical details and abbreviations. All the glasses were analysed with a 5-μm beam size

[b]Spinel compositions in reversal experiments rev2a–e were distinctly heterogeneous: the compositions listed in the table correspond to Sp analysed in the basaltic layer; Sp compositions in the peridotite layer have cr#'s larger by ≈5–8 units than those in the basaltic layer. In runs rev2f–g, Sp compositions were more homogeneous due to the large volume fraction of basalt and analyses of Sp grains from the upper part of the peridotite layer are included in the average

[c]The lines 'Ol, dike' and 'Sp, dike' give the compositions of Ol and Sp in the lower part of the basaltic microdike of sample #2

[d]Opx and Cpx were not analysed in sample rev2c

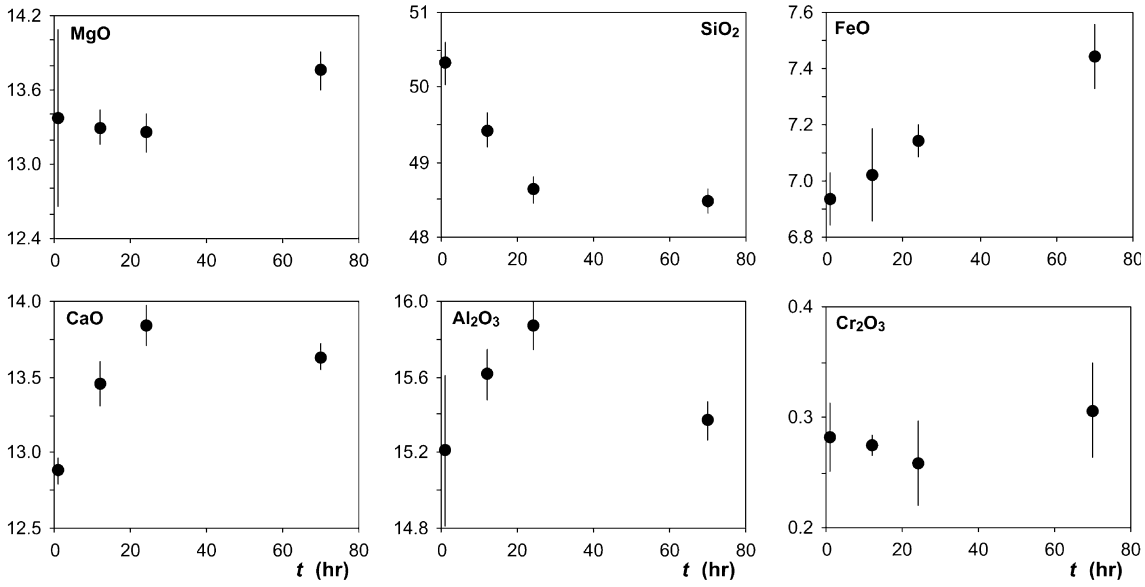

Fig. 6 Evolution of glass composition (in wt%) with run duration t (h) at 1300 °C

run #2 at 1,240 °C, however, significant differences are observed between the solid phases at the base of the microdikes and in the peridotite (Table 7). In particular, Sp in the basaltic microdike, is strongly depleted in Cr_2O_3 and enriched in Al_2O_3 (cr# = 10.7) compared with Sp in the peridotite (cr# = 28.0). Such compositional differences are rapidly eliminated at higher T: for example, in run #18 at 1,255 °C, Sp in the basaltic microdike is just slightly depleted in Cr_2O_3 and enriched in Al_2O_3 (cr# = 24.8) compared with Sp in the peridotite (cr# = 27.3).

Time-series experiments at 1,300 °C

To determine the timing of melt extraction into the microdikes, we performed three shorter duration experiments at 1,300 °C in addition to the 70-h run (#8; Table 2): #19 (1.0 h), #20 (12.0 h) and #22 (24.2 h). All three charges contained Ol, Opx, Sp and melt; thus, we deduce that all Cpx was consumed in the first hour of experiments at 1,300 °C. A microdike was observed in the three experiments, indicating that the fractures in the graphite lid formed early (presumably during the loading stage of the experiment) and were filled with liquid at the very beginning of the partial meting experiment.

Figure 6 shows the evolution of glass compositions with run duration increasing from 1 to 24.2 h: CaO, Al_2O_3 and FeO increase by 1, 0.7 and 0.2%, respectively; SiO_2 decreases by 1.7%. Interestingly, the evolutionary trends of most oxides reverse between 24.2 and 70 h: this is best seen in the CaO-, Al_2O_3- and MgO-time diagrams. No such reversals were observed in the chemical evolution of liquids extracted using the diamond aggregate techniques (Johnson and Kushiro 1992; Hirose and Kushiro 1993; Baker and Stolper 1994): in those studies, the concentrations of major elements reached nearly constant values after ≈24 h. Discussion of the time scales of chemical equilibration and a detailed analysis of the evolution of melt composition as a function of time will be presented below.

Reversal experiments

Reversal series rev6

In order to reverse partial melting experiment #6 (at 1,360 °C), we performed two sandwich experiments using gel B6 as the basalt component: rev6a at 1,375 °C and rev6b at 1,360 °C (pressure was 1 GPa in all the reversal experiments; Table 3). During these experiments, a large proportion of the basalt was dispersed by infiltration into the peridotite, such that the basaltic layer at the top of the sample was no longer identifiable at the end of the experiments. Two large, crystal-free glass pockets, about 200 μm in diameter, were, however, preserved in the upper corners of the sample chamber. In both experiments, the stable phases are Ol, Opx, Sp and liquid; Cpx is only found as quench overgrowths.

The relationships between phase compositions in runs #6, rev6a and rev6b may be summarised as follows (Table 5, Fig. 7):

1. Phase compositions in rev6b are close, but not identical to, the compositions in run #6. In particular, compared with glass #6, the glass in run rev6b is slightly depleted in MgO, FeO and SiO_2, and enriched in Al_2O_3, CaO, Na_2O and TiO_2. These features suggest that glass rev6b corresponds to a slightly smaller degree of melting of Depma than glass #6. For the solid phases, the mg#'s of Ol, Opx and Sp in runs #6 and rev6b are equal within error, but Sp has a distinctly smaller cr# in rev6b than in run #6.

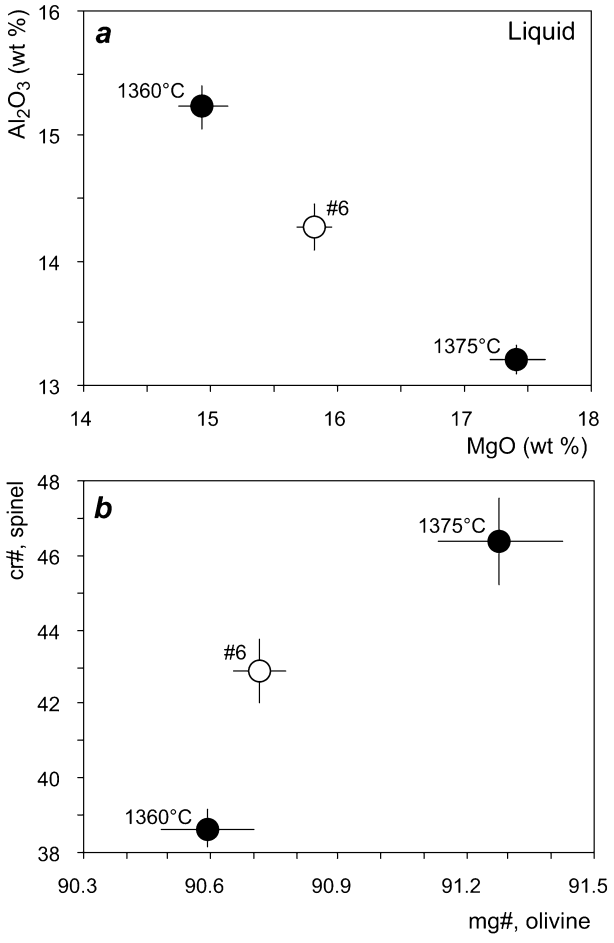

Fig. 7a–b A comparison of phase compositions in the partial melting experiment #6 (1,360 °C; *empty circle*) and in the reversal experiments rev6a and rev6b (*filled circles*); the temperature of the reversal experiments is indicated by the labels. **a** Plot of Al_2O_3 in glass as a function of MgO in glass. **b** Plot of cr# in Sp as a function of mg# in Ol

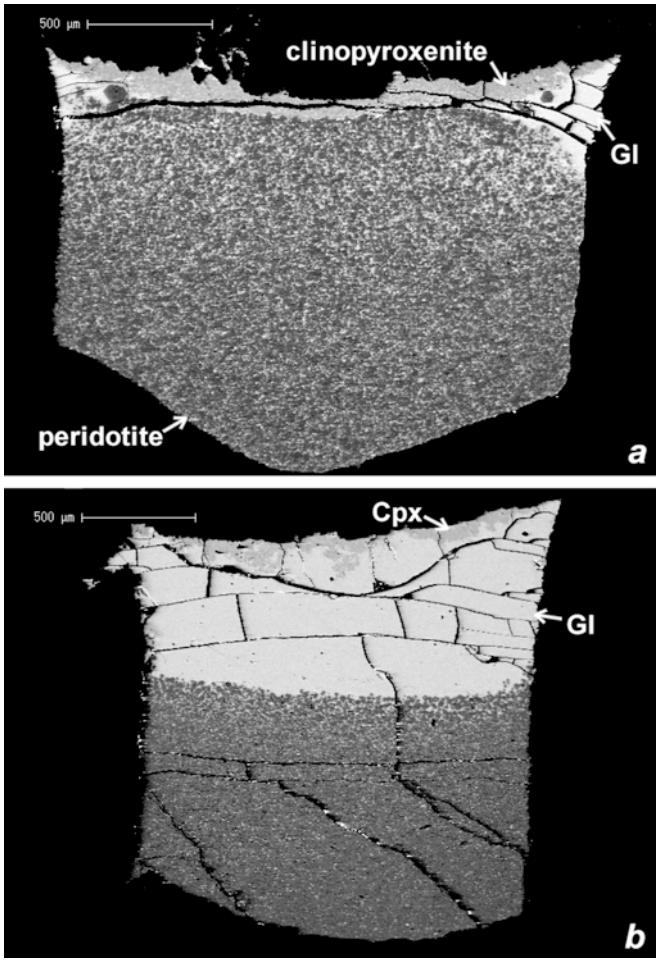

Fig. 8a–b Backscattered electron micrographs illustrating the internal structures in the reversal experiments. **a** Polished section of sample rev8b showing the lower peridotite layer, the upper clinopyroxenite layer and the glass pockets in the upper corners of the sample chamber. **b** Polished section of sample rev2a showing from the bottom to the top: the peridotite layer, a thick layer of glass and a thin layer of Cpx crystals hanging on the graphite lid. *Scale bars*: 500 μm

2. Important changes in phase compositions are observed with T increasing from 1,360 (rev6b) to 1,375 °C (rev6a): the concentrations of MgO, FeO, Cr_2O_3 and SiO_2 in the liquid phase increase while the concentrations of Al_2O_3, CaO, Na_2O and TiO_2 decrease significantly; for instance, MgO increases from 14.9 to 17.4% and Al_2O_3 decreases from 15.2 to 13.2%. For the solid phases, the most conspicuous variations concern mg# in Ol and Opx, and cr# in Sp: from 1,360 to 1,375 °C, mg# in Ol increases from 90.6 to 91.3, and cr# in Sp increases from 38.6 to 46.4.
3. For all major elements, the concentration in glass #6 is intermediate between the concentrations in glasses rev6a and rev6b. This result is illustrated in Fig. 7a for MgO and Al_2O_3. The same kind of relationship holds for the solid phases (Fig. 7b).

We conclude that the phase compositions in run #6 at 1,360 °C can be reversed at a temperature lying somewhere between 1,360 and 1,375 °C. The small difference (< 15 °C) between the temperature of the partial melting experiment and the temperature at which it can be reversed may result from the experimental T uncertainty. Alternatively, this temperature difference could be due to a slightly different water content in the direct melting experiment compared with the reversal experiments. As will be discussed in the next section, a difference in water content of the liquid of only 0.1–0.2% can be responsible for a T difference ≤ 15 °C.

Reversal series rev8

To reverse run #8 (at 1,300 °C), we first performed three sandwich experiments using nominally anhydrous basalt B8: rev8a at 1,300 °C, rev8b at 1,315 °C and rev8c at 1,330 °C (Table 3). Runs rev8a and rev8b show a layered structure comprising a lower layer of peridotite and

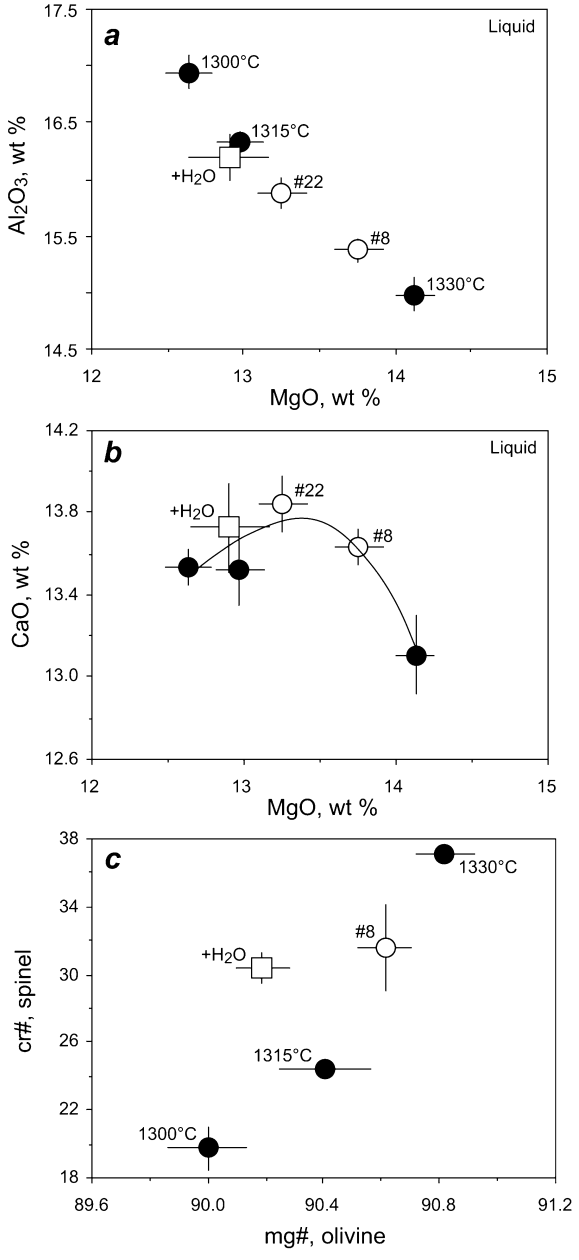

Fig. 9a–c A comparison of phase compositions in partial melting experiments #8 and #22 (both at 1,300 °C, but with different durations: 70 h for #8, 24.2 h for #22; *empty circles*), in reversal experiments rev8a-c (*filled circles*; T is indicated by the labels), and in reversal experiment rev8d (1,300 °C, 0.5% added water; *empty square*). Glass #22 is plotted in this figure to show that it corresponds to a very slightly lower degree of melting than #8 (see the text for further explanation). **a** Plot of Al_2O_3 in glass as a function of MgO in glass. **b** Plot of CaO in glass as a function of MgO in glass; to draw the compositional path of the liquid in the reversal experiments (*continuous line*), we assumed that a maximum CaO content was reached at the Cpx-out T (between 1,315 and 1,330 °C). **c** Plot of cr# in Sp as a function of mg# in Ol

an upper layer of clinopyroxenite (Fig. 8a); two large, three-sided glass pools are located at the upper corners of the sample chamber. The phases present within the peridotite are Ol, Opx, Sp and liquid; Cpx is abundant, but only as a quench product. The clinopyroxenite layer is 130 μm thick in rev8a and 100 μm thick in rev8b, by comparison, the original basalt layer was 500 to 600 μm thick, as computed from the mass of basalt B8. Accordingly, a large part of the basaltic layer was 'lost' by infiltration into the peridotite; basalt infiltration was responsible for the large melt fraction in the peridotite (from ≈30 vol% at the top of the peridotite layer to 10 vol% at the bottom, as compared with 5 vol% in run #8). Sample rev8c shows the same overall structure as samples rev8a–b except that there is no clinopyroxenite layer: the upper part of the sample is a discontinuous layer of glass pockets and large Ol grains, with no Cpx.

Phase compositions in runs rev8a–c are a strong function of T (Fig. 9; Table 6). From 1,300 to 1,330 °C, the concentrations of MgO, Cr_2O_3 and SiO_2 in the liquid phase increase while the concentrations of Al_2O_3 and Na_2O decrease. For almost all oxides, the concentration in glass #8 is intermediate between the concentrations in glasses rev8b and rev8c (Fig. 9a). Calcium shows a different behaviour: glasses rev8a–c have a smaller CaO content than glass #8. However, the compositional difference is quite small: the CaO content in glass rev8b is equal within error to the CaO content in glass #8. Interestingly, the Cpx-out T in the reversal experiments lies somewhere between 1,315 and 1,330 °C. We suggest that, at this temperature, the CaO content in the glass from the reversal experiments could reach a maximum value equal to or even higher than the CaO concentration in glass #8, as illustrated in Fig. 9b. Important compositional variations as a function of T are also observed in the solid phases (Fig. 9c). Again, Ol and Sp compositions in run #8 are intermediate between those in runs rev8b and rev8c.

At this point, our conclusions are that (1) phase compositions in run #8 cannot be reversed at the correct temperature, namely 1,300 °C and (2) phase compositions in rev8b–c, at 1,315 and 1,330 °C, are a good match with the compositions observed in run #8. The difference between the temperature of the partial melting experiment and the temperature at which it can be reversed, therefore, is slightly larger for run #8 than for run #6 (15–30 versus 0–15 °C). This 15–30 °C difference cannot be ascribed to the uncertainty in T associated with piston-cylinder experiments (the smooth compositional trends in Fig. 5 indicate that the precision in T in the present work is much better than ±15 °C). A possible explanation is that the liquid phase contained more dissolved water in run #8 than in runs rev8a–c. Reversal experiment rev8d was performed to test this hypothesis: it was run at 1,300 °C, but the added basalt contained 0.5% H_2O (Table 3). To accelerate the attainment of chemical equilibrium, the fraction of basalt was increased (51% as compared to 30–35% in rev8a–c) and part of the basalt was directly mixed with the peridotite powder.

The glass composition in rev8d is within error of that in experiment rev8b (Table 6; Fig. 9a, b). Mineral compositions in rev8b and rev8d are also almost identical except that (1) the Ol mg# is slightly lower (but still

within error) in rev8d than in rev8b and (2) the Sp cr# in rev8d is larger than in rev8b (and almost equal to cr# in run #8; Fig. 9c). The water content of glasses rev8b and rev8d was measured with an ion microprobe (Table 3). In the nominally anhydrous experiment rev8b, the water content is $0.28 \pm 0.02\%$; the water content in glass rev8d is $0.50 \pm 0.10\%$. From this set of data, we can draw the following conclusions:

1. The similarity of glass compositions in runs rev8b (1,315 °C; ≈0.3% H_2O) and rev8d (1,300 °C; ≈0.5% H_2O) shows that a 0.2% increase of the amount of water dissolved into the liquid is equivalent to a 15 °C temperature increase.
2. The addition of 0.5% H_2O to anhydrous basaltic composition B8 is not enough to allow run #8 to be reversed at 1,300 °C: from conclusion (1) above and Fig. 9, ~0.2% more water would be necessary to reproduce the phase compositions in run #8 in a reversal experiment at 1,300 °C. Therefore, the water content in glass #8 is estimated to be ≈0.7%. It was not possible to measure the water content of the glass in sample #8 directly by ion microprobe because the basaltic microdike was too thin. However, an ion microprobe spot in the larger basaltic microdike of sample #5 (1,285 °C; Fig. 4b) yielded a water content of 0.79%, in good agreement with our estimate for run #8.

Fig. 10a–f Plots of oxide concentrations in the liquid phase as a function of T for partial melting experiment #2 (1,240 °C; *empty circle*) and reversal experiments rev2a–e (*small solid circles* at 1,255 to 1,295 °C), rev2f (with 0.60% H_2O dissolved in the liquid phase; *small solid circle* at T = 1,240 °C), and rev2g (with 1.13% H_2O dissolved in the liquid phase; *large solid circle*). The composition of the added basalts in the reversal experiments is indicated by the *cross* (B2*, used in runs rev2f-g at 1,240 °C) and the horizontal line (B2, used in runs rev2a–e); composition B2* is not shown in **a**, **d** and **f** where it almost coincides to glass #2

Reversal series rev2

In order to reverse run #2 (at 1,240 °C), we first performed five experiments using the nominally anhydrous basalt B2: rev2a at 1,270 °C, rev2b at 1,280 °C, rev2c at 1,295 °C, rev2d at 1,255 °C and rev2e at 1,270 °C (Table 3). Samples rev2a–e showed a layered structure comprising, from the bottom to the top (Fig. 8b, Table 3), (1) a thick layer of partially molten peridotite, (2) a continuous glass layer, up to 650 μm thick and (3) a layer of clinopyroxenite hanging on the graphite lid (in run rev2c, only a few Cpx clusters are observed hanging on the graphite lid).

With increasing T, an important evolution of glass composition is observed in runs rev2a–e (Table 7, Fig. 10): the concentrations of MgO, FeO, CaO and Cr_2O_3 increase and the concentrations of Al_2O_3, SiO_2, Na_2O and K_2O decrease as T increases from 1,255 to 1,295 °C. MgO, Al_2O_3, Na_2O, FeO and TiO_2 in glass #2 are within the ranges of concentrations observed in the reversal experiments at 1,270 and 1,280 °C (rev2a–b, rev2e; Fig. 10); also, K_2O in glass #2 is equal within error to K_2O in glass rev2b. For three oxides, however, the concentrations in glass #2 are out of the range measured in glasses rev2a–e. (1) The CaO concentration in glasses rev2a–e increases from 10.4 to 11.4% with increasing T, but, even at 1,295 °C, it is still significantly lower than in glass #2 (11.9%). (2) SiO_2 concentrations in glasses rev2a–e are 0.5–1.3% larger than in glass #2. (3) Except at the lowest T (1,255 °C, rev2d), glasses rev2a–e have Cr_2O_3 concentrations about twice as large as in glass #2. From these results, we draw two preliminary conclusions.

1. The concentrations of most oxides in glass #2 are reproduced in the reversal experiments, but at 1,270–1,280 °C instead of 1,240 °C. As for series rev8, a simple explanation for this T discrepancy could be

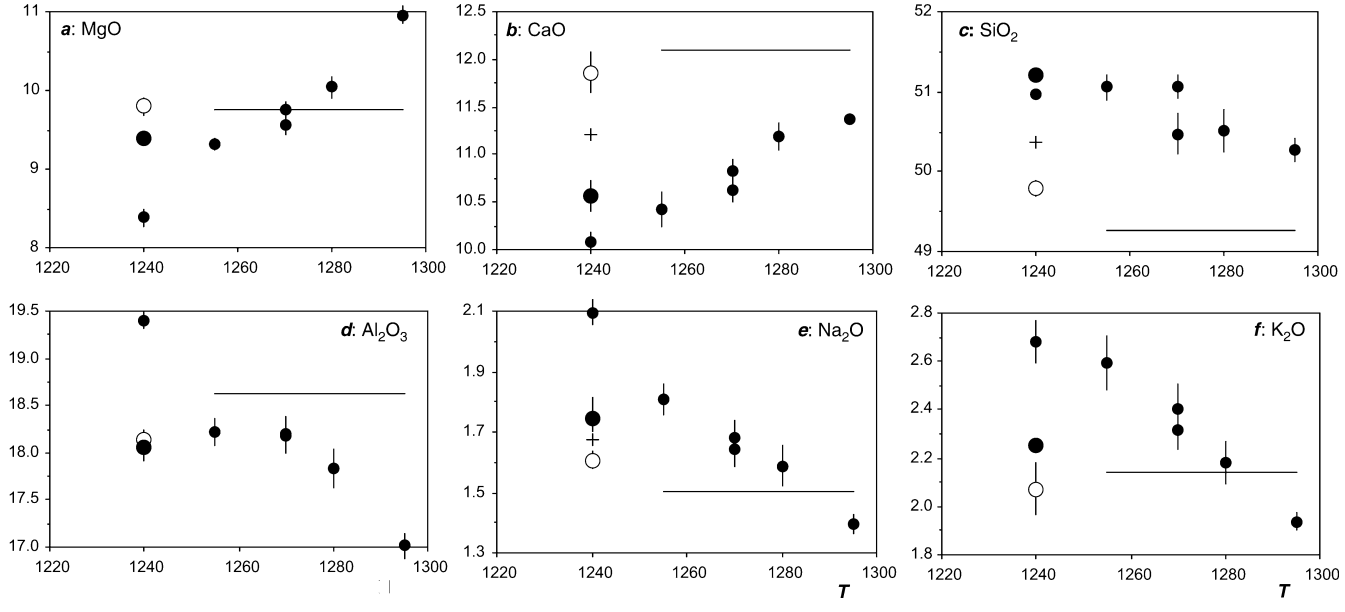

that the amount of water is larger in glass #2 than in glasses rev2a–e.

2. The glass composition analysed in the basaltic microdike of sample #2 is too rich in CaO and too poor in SiO_2 and Cr_2O_3 to be in equilibrium with Depma at the run conditions. The anomalously low Cr_2O_3 content of glass #2 explains why Sp in the basaltic microdike of sample #2 is strongly depleted in Cr_2O_3 compared with Sp in the peridotite (Table 7).

Reversal experiments, rev2f–g, were performed to test these two conclusions. Compared with glass #2, the basalt B2* used in these experiments contained less CaO (11.2% versus 11.9%; Table 1), more SiO_2 (50.4% versus 49.8%) and more Cr_2O_3 (0.10% versus 0.04%). The two experiments were run at 1,240 °C as #2, but the added basalt contained some dissolved water: 0.9% in run rev2f and 1.8% in run rev2g (Table 3). Compared with glass #2 and basalt B2*, glass rev2f is strongly enriched in incompatible elements (Na_2O, K_2O, Al_2O_3) and in SiO_2, and strongly depleted in compatible elements (MgO, FeO, Cr_2O_3 and CaO; see Fig. 10). These chemical features, combined with the thickness of the clinopyroxenite layer (170 μm; Table 3), indicate a relatively large degree of crystallisation of basalt B2*. A dramatic evolution of glass composition is observed with increasing water content (Fig. 10): for most elements (Na_2O, K_2O, Al_2O_3, MgO, FeO, Cr_2O_3, TiO_2), the concentrations in glass rev2g are very close or equal within error to the concentrations in B2*. The concentrations in CaO and SiO_2 in glass rev2g do not match, however, the concentrations in B2*: CaO is still ≈0.6% lower and SiO_2 ≈0.8% higher in rev2g than in B2*. Water contents of 0.60 ± 0.12% in glass rev2f and 1.13 ± 0.02% in glass rev2g were measured with an ion microprobe (Table 3; these values are 30–40% lower than the water contents in the starting basalt, presumably due to the escape of water into the graphite container). From Fig. 10, we estimate that an even better match of glass #2 for Na_2O, K_2O, Al_2O_3, MgO, FeO, Cr_2O_3, TiO_2 would have been obtained for a water content 0.1–0.2% larger than in rev2g.

Our conclusions are that (1) it is possible to reverse partial melting experiment #2 at the correct temperature (1,240 °C) provided the water content in the liquid is set to ≈1.2% and (2), under these conditions, the glass in equilibrium with Depma contains about 10.6% CaO, 51.2% SiO_2 and 0.1% Cr_2O_3 as compared with 11.9, 49.8 and 0.04%, respectively, in glass #2. Hereafter, glass rev2g is considered to be the best approximation for near-solidus melt compositions in Depma at 1 GPa. Finally, we stress that our estimate of ≈1.2% H_2O in glass #2 is a maximum because water may not be the only agent responsible for the T discrepancy between runs #2 and rev2a–e. Glass #2 is produced at a very low melt fraction (0.3%; Table 2), and is indeed enriched in incompatible trace elements; in particular, it contains significant amounts of P_2O_5 and Cl: 0.2 and 0.7%, respectively (Table 8). By comparison, melts in reversal experiments have negligible concentrations of these elements because they are derived from trace-element-free gels and because of the large melt fraction in the reversal experiments (P_2O_5 and Cl in reversal glass rev2c are below the detection limits of 0.01% for P_2O_5 and 0.02% for Cl). The enrichment in incompatible trace elements in glass #2 could be responsible for part of the 30–40 °C discrepancy between runs #2 and rev2a–e. From a parameterisation of the effect of phosphorus on peridotite solidus temperature (Wasylenki et al. 2003), we deduce that the temperature shift due to P_2O_5 in

Table 8 Cl, K_2O and P_2O_5 concentrations (wt%) in glasses and degrees of melting of the partial melting experiments[a]

		Cl[b]	K_2O[c]	P_2O_5	ϕ_{K2O}[d]	ϕ_{MB}[e]
#21[f]					0.15 (4)	0.18 (8)
#2	4	0.724 (7)	2.141 (8)	0.185 (4)	0.23 (5)	0.30 (12)
#18	8	0.218 (15)	0.652 (9)	0.148 (10)	0.77 (16)	0.97 (25)
#5	5	0.074 (12)	0.227 (2)	0.093 (8)	2.20 (46)	2.47 (42)
#11	6	0.082 (15)	0.255 (7)	0.101 (4)	1.96 (45)	2.29 (50)
#8	6	0.033 (8)	0.106 (6)	0.057 (7)	4.73 (119)	4.39 (54)
#17[f]					8.22 (464)	5.43 (90)
#6	6	0.029 (8)	0.071 (4)	0.039 (6)	7.04 (182)	6.50 (69)

[a]Cl, K_2O and P_2O_5 concentrations were determined by electron probe microanalysis (conditions: 10 kV, 100 nA and counting times of 20 s; beam size: 5–10 μm). The numbers in parentheses after the mean values are 1σ standard deviations, given in terms of the least unit cited. The number of analyses per sample is given in the second column

[b]The large Cl concentrations result presumably from trace quantities of insoluble chlorides left over after washing the mineral separates with dilute HCl (see Hirschmann et al. 1998). Cl concentration in Depma is only 15–20 ppm, however, as computed from the constant K_2O/Cl ratio in the glasses, $K_2O/Cl = 3.0$, and from K_2O concentration in Depma (0.005 ± 0.001 wt%; Table 1)

[c]K_2O abundances in partial melts are due to the relatively large K_2O concentration in Depma. MORBs are expected to be produced by 10% melting of mantle sources with ≈100 ppm K_2O (Hofmann 1988): even if one assumes incomplete melt extraction with 1–2% melt remaining stranded in the solid matrix, K_2O concentration in the residue should be at most 10–20 ppm, not 50 ppm as in Depma. The excess K_2O in Depma is presumably due to the presence of trace amounts of alteration products from abyssal peridotite KN3

[d]ϕ_{K2O} is the degree of melting (wt%) computed from the K_2O concentrations in glass and in peridotite Depma assuming a perfectly incompatible behaviour of potassium (that is, mineral–liquid partition coefficients, *Kd*, equal to zero for all solid phases). The large errors (in parentheses) are mostly due to the 20% relative error on the K_2O concentration in Depma; the large standard deviation of the K_2O concentration in glass #17 (33% relative) explains the anomalously large error on ϕ_{K2O}. For comparison, we computed ϕ_{K2O} using the *Kd*'s of Chen and Frey (1985), which yield a bulk partition coefficient of $\approx 5\times10^{-4}$: for all the experiments, but #21, #2 and #18, the results are almost indistinguishable from the values in the table; for #21, #2 and #18, the results are slightly lower than in the table, but still within error (0.11, 0.19 and 0.72 wt%, respectively)

[e]ϕ_{MB} is the degree of melting (wt%) computed by mass balance from bulk composition Depma and major element compositions of solid and liquid phases in the partial melting experiments

[f]Not analysed (due to the small thickness of the microdikes): ϕ_{K2O} in samples #21 and #17 was computed using the K_2O concentration in Table 4 (3.32 ± 23 and 0.06 ± 0.02 wt%, respectively)

our study is only ≈1 °C. The role of chlorine is presumably more important: the effect of Cl on degrees of melting in magmatic systems could be almost equivalent to the effect of water (Webster and McBirney 2001); also, the preferential association of Cl with Ca in the structure of aluminosilicate melts (Webster and De Vivo 2002) could explain, in part, the excess of calcium in glass #2. A detailed investigation of the effect of chlorine on peridotite melting is beyond the scope of this study.

Discussion

Degrees of melting in the partial melting experiments

Degrees of melting were computed by mass balance using two independent methods (Table 8). In the first method, the ten oxides in Table 4 were taken into account in the calculation: the proportions of liquid and solid phases best fitting bulk composition Depma were calculated using an algorithm that incorporates uncertainties in the phase and bulk compositions (Albarède and Provost 1977). The second method is a mass balance restricted to K_2O assuming that potassium is perfectly incompatible: the weight fraction of liquid, ϕ is calculated as a function of K_2O concentrations in liquid, $[K_2O]_{liquid}$, and in Depma, $[K_2O]_{bulk}$, through the relationship

$$\phi = [K_2O]_{bulk} / [K_2O]_{liquid}$$

Three major results emerge from Table 8:

1. Degrees of melting calculated by the two techniques are highly consistent and increase from 0.2% at 1,220 °C to ≈6.5% at 1,360 °C. Accordingly, the assumption that K_2O is perfectly incompatible is a good one (see footnote d in Table 8 for discussion). The data in Table 8 show that chlorine is also perfectly incompatible: the ratio K_2O/Cl is independent of melt fraction such that, in a diagram of K_2O (wt%) versus Cl (wt%), the data plot along a straight line (of slope 2.96; Fig. 11).
2. The microdike technique leads to separation of the liquid phase at extremely low degrees of melting: 1.0% in sample #18, 0.3% in sample #2 and 0.2% in sample #21 [in their clinopyroxenite melting experiments, Kogiso and Hirschmann (2001) described glass-filled cracks similar to our basaltic microdikes, but in samples with much larger degrees of melting: 5–6%].
3. The volume of liquid in the basaltic microdikes is only a small percentage of the total volume of liquid produced in the peridotite. From the shape and size of microdikes in cross section, the volume of segregated liquid is estimated to be as low as 0.001–0.01 mm^3. In comparison, the total volume of liquid produced ranges from 0.04 mm^3 in sample #2 to 0.9 mm^3 in sample #6 (as computed from the volume of peridotite, ≈12 mm^3 and the degrees of melting: 0.35 vol% in sample #2 and 7.6 vol% in sample #6). The implication is that some interstitial melt must be present within the peridotite in samples #21, #2 and #18 although no glass phase was detected in backscattered electron micrographs (Fig. 2a). Presumably, the resolution of back-scattered electron images (typically not better than a few tenths of a micron; Reimer 1998) does not allow the identification of melt unless the melt fraction exceeds a value lying somewhere between 1 and 2.5 vol% (Fig. 2b, c). Accordingly, care must be taken in determining solidus temperatures from textural arguments alone.

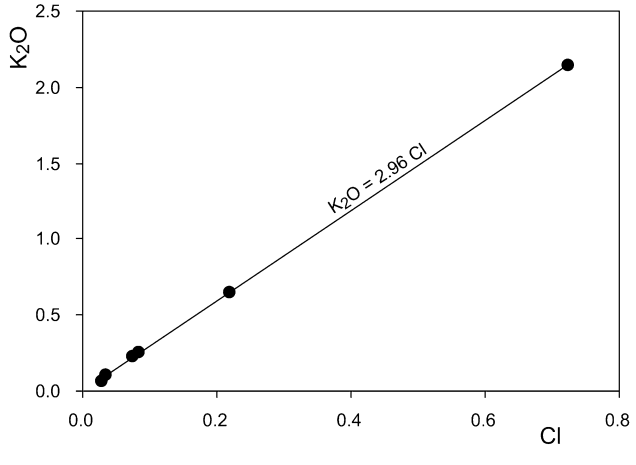

Fig. 11 Plot of K_2O (wt%) as a function of Cl (wt%) in partial melts

Length and time scales of chemical equilibration of liquids in partial melting experiments

Experiments at 1,300 °C

The structural and chemical observations in the time series at 1,300 °C point to the early extraction of a small volume of melt that was not at equilibrium (but not far from equilibrium) with peridotite Depma at run conditions. Chemical disequilibrium of the first formed melt is due to two main causes (Baker and Stolper 1994). First, all the mineral phases involved in peridotite melting are complex solid solutions whose compositions evolve with temperature: the first liquid formed must interact with the residual grains (by diffusion or dissolution-precipitation) such that chemical equilibrium cannot be established in the short time scale of melt extraction. Second, the solid phases may not melt in the correct (equilibrium) proportions due to variable melting kinetics. For instance, the higher SiO_2 and lower CaO concentrations in glass #19 (Fig. 6) could be due to an excessive contribution of Opx to the first formed melt.

With time, the segregated melt equilibrates with the partially molten peridotite, as indicated by the evolution of glass compositions with increasing run duration. Two processes must occur in parallel to achieve chemical equilibrium. First, the interstitial melt in the peridotite must re-equilibrate by dissolution and re-precipitation of the solid phases or by solid-state diffusion. Because solid-state diffusion is very sluggish, it is essential to use a very finely ground starting powder, as we did in these experiments. The second process involved is chemical diffusion between the segregated melt, which is not in intimate contact with the solid phases, and the melt in the partially molten peridotite. Effective diffusivities, D_{eff}, in a partially molten system are strongly reduced compared with diffusivities D_0 in the liquid because the liquid phase makes only a small volume fraction, ϕ_{V}, of the system (Dykhuizen and Casey 1989):

$$D_{\text{eff}} = D_0 \frac{\phi_{\text{V}}}{Z^2}$$

The tortuosity factor Z, accounts for the fact that channels in a partially molten system are not straight and parallel to the direction of transport ($Z^2 \approx 3$ for an isotropic pore network). Because both D_0 and ϕ_{V} decrease with decreasing temperature, it is clear from the above equation that the duration required for chemical equilibration will increase with decreasing degree of melting. In our kinetic series at 1,300 °C, melt fraction is ≈5 vol%. Considering values of D_0 in the range 10^{-10} to 10^{-11} m^2/s (values typical of Si in basaltic melt at 1,300 °C; Baker 1992; Lesher et al. 1996) and a time scale for diffusion $t = 70$ h, we computed effective diffusivities of 2×10^{-12} to 2×10^{-13} m^2/s and diffusion length scales ($\approx[D_{\text{eff}}\, t]^{1/2}$) of 200–600 μm. These length scales are smaller than the sample size, 2 mm, but the segregated melt was still able to interact and re-equilibrate with a reasonably large volume of partially molten peridotite over the time scale of the experiment.

The distinct reversals of the chemical trends for CaO, Al_2O_3, MgO and Cr_2O_3 between 24.2 and 70 h (Fig. 6) do not fit in the simple scenario of chemical equilibration depicted above: in a closed system at fixed pressure and temperature, oxide concentrations in the segregated melt should asymptotically approach constant values with time. By comparison with glass #22, glass #8 is slightly but systematically enriched in all compatible elements and depleted in incompatible elements such as Al_2O_3: therefore, it corresponds to a slightly larger degree of melting than glass #22. This larger degree of melting might simply result from a slightly larger effective T in run #8. From the slopes of oxide concentrations versus T in Fig. 5, a temperature difference of ≈15 °C could be responsible for the chemical differences between runs #8 and #22. Alternatively, the larger ϕ in run #8 could be due to the progressive diffusion of hydrogen into the capsule during the course of the experiment. An increase of the amount of water dissolved into the liquid of only 0.1–0.2% is enough to generate the chemical evolution from glass #22 to glass #8. Whatever the explanation, we stress that, for most oxides, glass compositions #8 and #22 are almost indistinguishable in Fig. 5: that is, the chemical variations at 1,300 °C with run duration increasing from 24.2 to 70 h are very small compared with the variations recorded from one T to another.

Experiments at very low degree of melting

The data in run #2 may be used to discuss the kinetics of melting and chemical equilibration at very low degree of melting. The exact composition of the first formed melt in run #2 is not known, but, by analogy with glass #2, we may anticipate that it was richer in CaO and poorer in SiO_2 and Cr_2O_3 than the equilibrium composition. Using Albarède and Provost's (1977) algorithm, we computed that one weight unit of liquid #2 can evolve to the equilibrium liquid composition (as approximated by the composition of glass rev2g) by crystallising 8% Cpx, 9% Ol and by dissolving 18% Opx. These crude calculations suggest that the Cpx fraction in the melting reaction was larger than the equilibrium value, the Opx fraction was smaller and that Ol (on the product side of the reaction for lherzolite melting at 1 GPa; Kinzler and Grove 1992) failed to crystallise in sufficient proportions. Upon re-equilibration with the partially molten peridotite, the segregated melt, therefore, should crystallise Cpx and Ol, and dissolve Opx. The abundance of Cpx grains in the crystalline roots of the basaltic microdikes (compare Figs. 2a and 4c) provides a strong argument for an excessive contribution of Cpx to melting in the low-T experiments.

The incomplete chemical equilibration at the end of run #2 is presumably due to the very low effective diffusivities in the partially molten peridotite: values of D_{eff} in run #2 were about 30 times smaller than in run #8 because of the effect of temperature on D_0 and of the much smaller volume fraction of melt (0.0035 versus 0.051). In comparison, the duration of run #2 was only twice that of run #8. As a result, the diffusion length scale in run #2 was four times shorter than in run #8:50–150 μm instead of 200–600 μm. Qualitatively, this very short length scale means that the segregated liquid was not able to interact with a sufficient volume of partially molten peridotite to fully erase the initial chemical disequilibrium.

Concentrations and origin of water in the partial melting experiments

The ion microprobe analyses provide us with a quantitative measure, not only of the water contents in the liquid phase, H_2O_{liquid}, but also the bulk water contents, H_2O_{bulk}, of several samples (reported in Table 9). Despite our efforts to keep the starting powder and the

Table 9 Water contents in the liquid, H_2O_{liquid} (in wt%), and bulk water contents, H_2O_{bulk} (in ppm), of a few samples as a function of melt fraction, ϕ_{MB} (in wt%)

Sample	ϕ_{MB}[a]	H_2O_{liquid}[b]	H_2O_{bulk}[c]	Model[d]
#2	0.3	(1.2)	130 (30)	1.78
#5	2.47	0.79	250 (50)	0.79
#8	4.39	(0.7)	350 (60)	0.53
rev8b	27.79	0.28 (2)	800 (80)	0.11

[a]See Table 8 for the computation of ϕ_{MB}

[b]Water content in glass #5 was measured with an ion microprobe (one analytical spot); water content in glass rev8b is from Table 3. Water contents in glasses #2 and #8 were estimated on the basis of water contents measured in reversal glasses rev2g and rev8d, respectively (see text for further explanation)

[c]The bulk water content in a sample was computed using the mass-balance equation (e.g. Albarède and Provost 1977): $H_2O_{bulk} = H_2O_{liquid}\left[x_{liquid} + \sum_i x_i Kd_i\right]$ where x_{liquid} is the mass fraction of liquid ($=\phi_{MB}$), x_i is the mass fraction of solid phase i in the sample and Kd_i is the partition coefficient of water between solid phase i and liquid. Following Stolper and Newmann (1994), we used mineral/liquid partition coefficients close to the values for La and yielding a bulk partition coefficient of ≈0.01; x_{liquid} and the x_i's were computed by mass balance on the ten major and minor elements in Table 4

[d]Water contents in the liquid (wt%) for a fertile mantle source containing 300 ppm water, at degrees of melting of 0.3, 2.47, 4.39 and 27.79%; water contents were computed using Eq. 15 in Shaw (1970) with D_0 and P set to 0.014 and 0.038, respectively. Model assumes that mantle mineralogy if 0.50 Ol + 0.30 Opx + 0.17 Cpx + 0.03 Sp, and that the melting reaction is 0.7 Cpx + 0.4 Opx + 0.1 Sp = 1. 0 liquid + 0.2 Ol (Baker and Stolper 1994)

parts of the piston-cylinder assemblies dry, the experimental glasses contain amounts of water in the range 0.2–0.3 to 1.2%. These values are comparable to the water concentrations measured in the glasses of most nominally anhydrous, mantle melting experiments (Gaetani and Grove 1998; Hirschmann et al. 1998; Falloon et al. 2001; Wasylenki et al. 2003). The data in Table 9 show that both H_2O_{liquid} and H_2O_{bulk} are systematic functions of melt fraction ϕ. For example, with ϕ increasing from 0.3% (sample #2) to 27.8% (sample rev8b), H_2O_{bulk} increases from 130 to 800 ppm. The variability of H_2O_{bulk} implies that part of the water was gained during the experiment (by diffusion of hydrogen through the platinum capsule); this result is consistent with the evolution of glass composition observed between 24.2 and 70 h in the time-series experiments at 1,300 °C. The relation between ϕ and H_2O_{bulk} also implies that the access of water is promoted by a large melt fraction. Quantitatively, however, H_2O_{bulk} increases by only a factor 6 for a factor 100 increase in melt fraction: as a result, the water content of the liquid phase decreases while the bulk water content increases. Therefore, it is more difficult to approach near-anhydrous conditions in experiments with a low melt fraction because contamination by only trace amounts of water can readily yield water contents in the liquid of several tenths of a per cent to 1%. This conclusion is consistent with the fact that the temperature discrepancy between the reversal experiments and the direct partial melting experiments increases with decreasing ϕ: 0–10 °C for run #6 (1,360 °C), 15–30 °C for run #8 (1,300 °C) and 30–40 °C for run #2 (1,240 °C).

Finally, we want to stress that, with H_2O contents of 100–450 ppm in MORB mantle sources (Michael 1988; Sobolev and Chaussidon 1996), natural partial melts formed at degrees of melting of < 1% to a few per cent ought to contain significant amounts of dissolved water. For $H_2O_{bulk} = 300$ ppm, for instance, H_2O_{liquid} will exceed 0.5% for all degrees of melting lower than ≈5% (Table 9; fortuitously, the values of H_2O_{liquid} in our partial melting experiments are close to those expected in a fertile mantle source with $H_2O_{bulk} = 300$ ppm). The importance of water to mantle melting at mid-ocean ridges has recently been emphasised by Asimow and Langmuir (2003).

Implications for the influence of water during mantle melting

Previous experimental studies have shown that water has a major effect on the melting relations of peridotite (Kushiro 1969; Stolper and Newman 1994; Hirose and Kawamoto 1995). First, it lowers the solidus temperature and it increases the degree of melting at a given T compared with dry peridotite. Second, it changes the stoichiometry of melting reactions and, therefore, the compositions of partial melts (Gaetani and Grove 1998). However, these previous studies were devoted to large water contents or to melting relations at water saturation, so direct comparison with the results of our experiments at small water contents can only be made in qualitative or semiquantitative terms.

A comparison of the Cpx-out T and of glass compositions in the direct melting experiment #8 and in the reversal experiments rev8a–c demonstrates that the main effect of a small amount of water is to increase the degree of melting at a given T (water content is ≈0.4% larger in glass #8 than in glasses rev8a–c; Table 9): (1) Cpx disappears between 1,290 and 1,300 °C in the partial melting experiments whereas it disappears between 1,315 and 1,330 °C in reversal series rev8; and (2) both experiments #8 and rev8a were run at 1,300 °C, but the glass in rev8a has distinctly lower concentrations in compatible elements and higher concentrations of incompatible elements than glass #8 (Fig. 9a). The addition of a small amount of H_2O, therefore, would not appear to displace the Ol + Opx + Sp cotectic significantly in compositional space. For all elements in Table 6, glass #8 is intermediate between glasses rev8b and rev8c (at 1,315 and 1,330 °C, respectively); in other words, adding a small amount of H_2O (here, + 0.4% in the liquid) is merely equivalent to increasing T (here, by ≈25 °C).

This conclusion contrasts somewhat with studies at higher water contents, which have shown that the addition of large amounts of water significantly changes the stoichiometry of peridotite melting reactions

(Gaetani and Grove 1998). According to Gaetani and Grove, these changes are primarily due to the effect of T on the compositions of coexisting pyroxenes. Their hydrous melting experiments were run at temperatures ≈100 °C lower than their dry experiments, so the CaO content of Cpx was much larger in the hydrous than in the dry experiments (for instance, 19.1% in run B304 at 1.2 GPa, 1,215 °C and $H_2O_{liquid} = 6.0\%$ versus 13.8% in run B303 at 1.2 GPa, 1345 °C and $H_2O_{liquid} = 0.7\%$). In comparison, our range of Cpx compositions, even in experiments based upon run #2 where the temperature shift was greatest, is much more restricted: from ≈18–19% CaO at 1,240 °C to ≈16.5% CaO at 1,280 °C (Table 7), explaining why we do not infer an important effect of a small amount of water on the Ol + Opx + Cpx + Sp cotectic. Consequently, we predict that, in a truly dry system, the chemical trends in Fig. 5 should remain essentially unchanged, except for a shift and a shortening of the T scale from 1,220–1,360 to ~1,280–1,370 °C.

Experimental determination of the mantle solidus

Significant experimental efforts have been expended to determine the solidus temperature of mantle assemblages (e.g. Hirschmann 2000). When compared with the dry solidus of less refractory peridotites at 1 GPa (1,240–1,270 °C; Baker et al. 1995; Falloon et al. 1999; Pickering-Witter and Johnston 2000; Schwab and Johnston 2001; Wasylenki et al. 2003), we find that our solidus is significantly lower (≤ 1,220 °C), a surprising result at first glance. However, as argued above, partial melting at a T as low as 1,220 or 1,240 °C was made possible by the presence of trace amounts of water in our experiments. If we take into account the 30–40 °C shift measured for the near-solidus experiment #2 at 1,240 °C, the corrected solidus falls in the range 1,270–1,280 °C, in very good agreement with the nominally-anhydrous solidus of depleted mantle composition DMM1, 1,250–1,270 °C (Wasylenki et al. 2003; DMM1 is slightly less refractory than Depma).

It is also important to emphasise that solidus temperatures in our study and in previous studies are not directly comparable because they were determined using different techniques. Solidus temperatures in the literature are deduced from the observation of backscattered electron micrographs of the peridotite or by computing the zero-ϕ intercept of a ϕ versus temperature curve (in which the minimum value of ϕ is usually 2% or more; e.g. Pickering-Witter and Johnston 2000): these techniques are not appropriate to detect a low-ϕ tail due to trace amounts of water, as observed in our study (Fig. 3). For instance, the solidus T of Depma at 1 GPa would lie between 1,270 and 1,285 °C on the basis of backscattered electron micrographs (runs #3 and 5, respectively; see section Degrees of melting in the partial melting experiments). If the zero-ϕ intercept technique is applied to our experiments in the T range 1,285–1,300 °C, we obtain a solidus T of ≈1,270 °C. Accordingly, the apparent difference in solidus temperature between our study and previous studies might simply be due to our ability to detect vanishingly small degrees of melting owing to the development of basaltic microdikes.

Comparing techniques to characterise low-degree mantle melts

In the last 10 years, systematic experimental studies using aggregates of diamonds (Baker and Stolper 1994; Baker et al. 1995) or vitreous carbon spheres (Wasylenki 1999; Pickering-Witter and Johnston 2000; Schwab and Johnston 2001; Wasylenki et al. 2003) have provided a much better understanding of peridotite melting. Wasylenki et al. (2003) demonstrated that liquids extracted into aggregates of vitreous carbon spheres approached equilibrium closely at melt fractions as low as 2%. The main difference between extraction techniques involving diamonds or vitreous carbon spheres and the microdike technique is that there is no pre-existing trap in the latter: the trap is created by the fracture of the graphite lid at the beginning of the experiment. Another important difference is that the volume of segregated liquid is very small: 0.001–0.01 mm^3, only 0.01–0.1% of the total peridotite volume (12 mm^3). In comparison, the minimal volume of the porous space in a diamond aggregate is equal to ≈1% of the peridotite volume (Hirose and Kushiro 1993). Accordingly, an advantage of the microdike technique is that it is particularly well suited to the study of mantle melting at very low melt fractions: down to ≈0.2%.

According to Falloon et al. (1999), the sandwich technique, rather than an extraction technique such as the diamond-aggregate technique, should be used to determine the composition of low-degree mantle melts. The advantage of the sandwich configuration is that a large area of glass unaffected by the crystallisation of quench products can be analysed (Stolper 1980; Takahashi and Kushiro 1983; Falloon and Green 1987; Robinson et al. 1998). The major drawback of this technique is that the final glass composition depends strongly on the composition of the added basalt and on the ratio basalt/(basalt + peridotite) of the sandwich. Accordingly, the sandwich technique is not really appropriate to the determination of the equilibrium melt composition in a specific peridotite source, except if the two following conditions are satisfied: (1) the volume of added basalt is small compared with the volume of liquid formed in the peridotite (a condition difficult to satisfy at low degrees of melting); and (2) the composition of the added basalt is as close as possible to the equilibrium melt composition of the peridotite at the P and T of interest, implying some prior independent knowledge of that composition.

However, one purpose for which sandwich experiments can be very useful, is to check whether the liquid composition determined using an extraction technique in a direct partial melting experiment is the equilibrium composition or not. Falloon et al. (1999) made multiple saturation and sandwich experiments to reverse the results of Baker and Stolper (1994). Combining their study and our own reversal experiments, it seems possible to make the following generalisations:

1. Extraction techniques work perfectly well at high temperatures and/or high degrees of melting: runs #26 of Baker and Stolper (1,390 °C, $\phi = 27.4\%$) and #6 of this study (1,360 °C, $\phi = 6.5\%$) were reversed within 0–10 °C of the direct partial melting experiments.
2. At lower temperatures, a partial melting experiment at a given T can only be reversed at a slightly larger temperature, T + ΔT, where ΔT increases with decreasing T or degree of melting. These temperature shifts do not mean that the segregated glasses are out of equilibrium: They simply result from the fact that liquids produced at very low degrees of melting are enriched in incompatible components (H_2O, P_2O_5, Cl, etc.), which are not incorporated in the basalts used in reversal experiments. Ideally, the concentrations of these components in the segregated glasses should be measured and a basalt with the same concentrations should be used in the sandwich experiments.
3. At very low melt fractions, some degree of chemical disequilibrium between the segregated liquid and the peridotite may persist even after 4–5 days. Depending on grain size and melt fraction, the incomplete chemical equilibration may be due to either the very slow rates of solid-state diffusion in the crystals or to the very low effective diffusivities of a partially molten system when ϕ is reduced to <1 to a few vol%. However, by combining the sandwich technique and an extraction technique (to tightly constrain the starting composition of the basalt glass in the sandwich), it is possible to closely approach the equilibrium composition of partial melts at degrees of melting of only a few tenths of a per cent. A corollary of our experiments is that a natural mineral mix is a suitable starting material for partial melting experiments provided its grain size has been reduced to a few micrometres to shorten the time scale of chemical equilibration.

Implications for partial melting of a depleted mantle

By comparison with a fertile peridotite such as MM3 (Baker and Stolper 1994), Depma is characterised by lower modal abundances of Cpx and Sp, and by the very low compositional fertility of these two phases: as a result, its concentrations in CaO, Al_2O_3, TiO_2 and Na_2O (1.20, 1.86, 0.02, and 0.02%, respectively) are much lower than in MM3 (3.57, 3.98, 0.11 and 0.31%). The effects of chemical depletion on the phase relations of peridotite, melt productivity and melt compositions may be summarised as follows:

1. The absence of plagioclase in runs #21 and #2, in which melt fraction is ≈0%, indicates that plagioclase is not stable at the 1-GPa solidus of Depma. In an ongoing experimental series at 0.5 GPa, about 1% plagioclase ($An_{90\text{-}95}$) grew from mineral mix Depma at solidus T (1,205 °C). Accordingly, the maximum pressure at which plagioclase is stable as a subsolidus phase in Depma lies somewhere between 0.5 and 1.0 GPa. In comparison, plagioclase is stable up to 1.3 GPa in fertile composition MM3 (Falloon et al. 1999).
2. Reaction temperatures (solidus T, Cpx-out T) and source fertility are strongly sensitive to the modal abundance of Cpx (see also Wasylenki et al. 2003). For instance, the melt fraction at Cpx-out T increases from 3–4% in Depma, which contains only 3.5% Cpx, to ≈20% in MM3 (which contains 17% Cpx; Baker and Stolper 1994). In terms of T, the effects of decreasing Cpx abundance are to increase solidus temperatures and to decrease Cpx-out temperatures. From MM3 to Depma, solidus T increases from ≈1,240 to 1,280 °C (Depma solidus is corrected for the effect of H_2O as discussed above) and Cpx-out T decreases from 1,330–1,350 to 1,290–1,300 °C.
3. At a given MgO concentration, SiO_2 is about 2 wt% lower in Depma liquids than in MM3 liquids. Depma liquids are, however, more silica-saturated than MM3 liquids because they have much lower Na_2O concentrations: normative Ol contents are ≈0-7 mol% lower and normative hyperstene (Hy) contents are 5–10 mol% higher in Depma than in MM3 liquids. In addition, near-solidus liquids from Depma are Hy-normative, not nepheline-normative as near-solidus liquids from MM3 (Falloon et al. 1999). For instance, glass rev2g, which is the best proxy for the first liquid produced from Depma, has 9.7 mol% normative Hy. Accordingly, a major effect of chemical depletion in spinel lherzolites is to displace the near-solidus melts from the alkali-basalt field of the basalt tetrahedron to the Ol tholeiite field, a result already well established in the system $CaO–MgO–Al_2O_3–SiO_2–Na_2O$ (Walter and Presnall 1994).
4. Glass compositions show a distinct enrichment in SiO_2 at low degrees of melting (Fig. 5). Enrichment in SiO_2 in near-solidus melts is well documented in fertile peridotites (Baker et al. 1995; Robinson et al. 1998) and is due to the effect of alkalies on the structure of silicate liquids and on the activity coefficient of silica in liquid. The liquid produced by ≈2% melting of MM3 at 1 GPa has 55.5% SiO_2 and 7.8% $Na_2O + K_2O$ (Hirschmann et al. 1998). Silica enrichment in our experiments is not as pronounced

due to the lower concentrations in alkali oxides: SiO_2 increases from 48–49% at melt fractions of ≈1% or more to a maximum value of 51.2% in glass rev2g ($Na_2O + K_2O = 4.0\%$; Table 7). Specific features of our study are that SiO_2 enrichment becomes detectable only at degrees of melting of a few 0.1% and that it is associated with very large values of K_2O (≥2%; Fig. 5).

Conclusions

The new 'microdike' melt extraction technique presented here is shown to be capable of separating small volumes of liquid from a partially molten peridotite assemblage. Compared with other melt extraction techniques, the main advantage of our approach is that microdike volume is only 0.01–0.1% of the total peridotite, such that degrees of melting much lower than 1% can be studied. However, we note that, at very low degrees of melting, the composition of the segregated liquid may deviate to some extent from the equilibrium composition: at these low degrees of melting, the sandwich technique must be used to check whether segregated liquids are at equilibrium and, if not, to approach more closely the equilibrium composition. Another important conclusion of this study is that more systematic measurements of the amounts of water dissolved in the segregated glasses, as well as detailed investigations of the effect of small water contents on liquidus temperatures and phase compositions, are necessary. Such considerations may provide a simple explanation for discrepancies between extraction experiments and sandwich experiments. Finally, we emphasise that, in nature, mantle melts formed at degrees of melting of $< 1\%$ to a few per cent are expected to contain significant amounts of dissolved water (Table 9): accordingly, the ultimate experimental goal should not be to work under perfectly anhydrous conditions, but rather to work at a constant bulk water content of the peridotite.

Acknowledgements This study has benefited from discussions with Etienne Médard, Pierre Schiano, Edward Stolper and Daniel Vielzeuf. Special thanks are due to the following persons and services: Ariel Provost for his mass-balance program; Pierre Boivin for his CIPW-norm program and for much technical advice; Michèle Veschambre for technical assistance with the electron probe microanalysis; Etienne Deloule for ion microprobe analyses; Catherine Mével for launching this research program; Christiane Wagner and Michel Fialin for measuring the ratio $Fe^{3+}/(Fe^{2+} + Fe^{3+})$ in glass rev8c; Antoine Bézos and Eric Humler for providing a piece of JDF-D2 MORB glass standard; and the Service d'Analyse des Roches et Minéraux (CRPG, Nancy) for the ICP-AES analyses in Table 1. The manuscript was improved by the careful reviews of Dana Johnston and Marc M. Hirschmann. This research program was supported by the Institut National des Sciences de l'Univers (INSU-CNRS), through grant 98-Dorsales-02 and in part by the European Community's Human potential Programme under contract HPRN-CT-2002-00211 [Euromelt]. Contribution INSU-CNRS 343.

References

Albarède F, Provost A (1977) Petrologic and geochemical mass-balance equations: an algorithm for least-square fitting and general error analysis. Computers Geosci 3:309–326

Asimow PD, Langmuir CH (2003) The importance of water to oceanic mantle melting regimes. Nature 421:815–820

Auzende JM, Cannat M, Gente P, Henriet JP, Juteau T, Karson J, Lagabrielle Y, Tivey MA (1993) Deep layers of mantle and oceanic crust exposed along the southern wall of the Kane Fracture Zone: submersible observations. Comptes Rendus Acad Sci Paris 317:1641–1648

Baker DR (1992) Estimation of diffusion coefficients during interdiffusion of geologic melts: application of transition state theory. Chem Geol 98:11–21

Baker MB, Stolper EM (1994) Determining the composition of high-pressure mantle melts using diamond aggregates. Geochim Cosmochim Acta 58:2811–2827

Baker MB, Hirschmann MM, Ghiorso MS, Stolper EM (1995) Compositions of near-solidus peridotite melts from experiments and thermodynamic calculations. Nature 375:308–311

Boettcher AL, Windom KE, Bohlen SR, Luth RW (1981) Low-friction, anhydrous, low- to high-temperature furnace sample assembly for piston-cylinder apparatus. Rev Sci Instrum 52:1903–1904

Cawthorn RG, Ford CE, Biggar GM, Bravo MS, Clarke DB (1973) Determination of the liquid composition in experimental samples: discrepancies between microprobe analysis and other methods. Earth Planet Sci Lett 21:1–5

Chen CY, Frey FA (1985) Trace element and isotopic geochemistry of lavas from Haleakala volcano, East Maui, Hawaii: implications for the origin of Hawaiian basalts. J Geophys Res 90:8743–8768

Deloule E (2002) Measuring D/H ratio of femtograms of hydrogen by ion microprobe: limits and applications. Geochim Cosmochim Acta 66(abstr):A175

Deloule E, Paillat O, Pichavant M, Scaillet B (1995) Ion microprobe determination of water in silicate glasses: methods and applications. Chem Geol 125:19–28

Draper DS, Green TH (1999) P–T phase relations of silicic, alkaline, aluminous liquids: new results and applications to mantle melting and metasomatism. Earth Planet Sci Lett 170:255–268

Dykhuizen RC, Casey WH (1989) An analysis of solute diffusion in rocks. Geochim Cosmochim Acta 53:2797–2805

Falloon TJ, Green DH (1987) Anhydrous partial melting of MORB pyrolite and other peridotite compositions at 10 kbar: implications for the origin of primitive MORB glasses. Mineral Petrol 37:181–219

Falloon TJ, Green DH, Danyushevsky LV, Faul UH (1999) Peridotite melting at 1.0 and 1.5 GPa: an experimental evaluation of techniques using diamond aggregates and mineral mixes for determination of near-solidus melts. J Petrol 40:1433–1375

Falloon TJ, Danyushevsky LV, Green DH (2001) Peridotite melting at 1 GPa: reversal experiments on partial melt compositions produced by peridotite–basalt sandwich experiments. J Petrol 42:2363–2390

Fialin M, Wagner C, Métrich N, Humler E, Galoisy L, Bézos A (2001) Fe3+/ΣFe vs. FeLα peak energy for minerals and glasses: recent advances with the electron microprobe. Am Mineral 86:456–465

Gaetani GA, Grove TL (1998) The influence of water on melting of mantle peridotite. Contrib Mineral Petrol 131:323–346

Ghose I, Cannat M, Seyler M (1996) Transform fault effect on mantle melting in the MARK area (Mid-Atlantic Ridge south of Kane transform). Geology 24:1139–1142

Hirose K, Kawamoto T (1995) Hydrous partial melting of lherzolite at 1 GPa: the effect of H_2O on the genesis of basaltic magmas. Earth Planet Sci Lett 133:463–473

Hirose K, Kushiro I (1993) Partial melting of dry peridotites at high pressures: determination of compositions of melts segre-

gated from peridotite using aggregates of diamond. Earth Planet Sci Lett 114:447–489
Hirschmann MM (2000) Mantle solidus: experimental constraints and the effects of peridotite composition. Geochem Geophys Geosyst 1. Paper number 2000GC000070
Hirschmann MM, Baker MB, Stolper EM (1998) The effect of alkalis on the silica content of mantle-derived melts. Geochim Cosmochim Acta 62:883–902
Hofmann AW (1988) Chemical differentiation of the Earth: the relationship between mantle, continental crust, and oceanic crust. Earth Planet Sci Lett 90:297–314
Johnson KTM, Kushiro I (1992) Segregation of high-pressure partial melts from peridotite using aggregates of diamond: a new experimental approach. Geophys Res Lett 19:1703–1706
Johnson KTM, Dick HJB, Shimizu N (1990) Melting in the oceanic upper mantle: an ion microprobe study of diopsides in abyssal peridotites. J Geophys Res 95:2661–2678
Kinzler RJ, Grove TL (1992) Primary magmas of mid-ocean ridge basalts. 1. Experiments and methods. J Geophys Res 97:6885–6906
Kogiso T, Hirschmann MM (2001) Experimental study of clinopyroxenite partial melting and the origin of ultra-calcic melt inclusions. Contrib Mineral Petrol 142:347–360
Kushiro I (1969) The system forsterite–diopside–silica with and without water at high pressures. Am J Sci Schairer 267-A:269–294
Langmuir CH, Klein EM, Plank T (1992) Petrological systematics of mid-ocean ridge basalts: constraints on melt generation beneath ocean ridges. In: Phipps Morgan J, Blackman DK, Sinton JM (eds) Mantle flow and melt generation at mid-ocean ridges. Am Geophys Union Geophys Monogr 71:183–280
Lesher CE, Hervig RL, Tinker D (1996) Self diffusion of network formers (silicon and oxygen) in naturally occurring basaltic liquid. Geochim Cosmochim Acta 60:405–413
Michael PJ (1988) The concentration, behaviour and storage of H_2O in the suboceanic upper mantle: implications for mantle metasomatism. Geochim Cosmochim Acta 52:555–566
Michael PJ, Schilling JG (1989) Chlorine in mid-ocean ridge magmas: evidence for assimilation of seawater-influenced components. Geochim Cosmochim Acta 53:3131–3143
Pickering-Witter J, Johnston AD (2000) The effects of variable bulk composition on the melting systematics of fertile peridotitic assemblages. Contrib Mineral Petrol 140:190–211
Reimer L (1998) Scanning electron microscopy: physics of image formation and microanalysis. Springer series in optical sciences, vol 45, 2nd edn. Springer, Berlin Heidelberg New York
Reynolds JR, Langmuir CH (1997) Petrological systematics of the mid-Atlantic ridge south of Kane: implications for ocean crust formation. J Geophys Res 102:14915–14946
Robinson JAC, Wood BJ, Blundy JD (1998) The beginning of melting of fertile and depleted peridotite at 1.5 GPa. Earth Planet Sci Lett 155:97–111
Schiano P, Bourdon B, Clochiatti R, Massare D, Varela ME, Bottinga Y (1998) Low-degree partial melting trends recorded in upper mantle minerals. Earth Planet Sci Lett 160:537–550
Schwab BE, Johnston AD (2001) Melting systematics of modally variable, compositionally intermediate peridotites and the effects of mineral fertility. J Petrol 42:1789–1811
Shaw DM (1970) Trace element fractionation during anatexis. Geochim Cosmochim Acta 34:237–243
Smith CS (1964) Some elementary principles of polycrystalline microstructure. Metall Rev 9:1–48
Sobolev AV, Chaussidon M (1996) H_2O concentrations in primary melts from supra-subduction zones and mid-ocean ridges: implications for H_2O storage and recycling in the mantle. Earth Planet Sci Lett 137:45–55
Stolper E (1980) A phase diagram for mid-ocean ridge basalts: preliminary results and implications for petrogenesis. Contrib Mineral Petrol 74:13–27
Stolper E, Newman S (1994) The role of water in the petrogenesis of Mariana trough magmas. Earth Planet Sci Lett 121:293–325
Takahashi E, Kushiro I (1983) Melting of a dry peridotite at high pressures and basalt magma genesis. Am Mineral 68:859–879
Walter MJ, Presnall DC (1994) Melting behavior of simplified lherzolite in the system $CaO–MgO–Al_2O_3–SiO_2–Na_2O$ from 7 to 35 kbar. J Petrol 35:329–359
Wasylenki LE (1999) Partial melting of depleted peridotite in the earth's upper mantle and implications for generation of mid-ocean ridge basalts. PhD Thesis, California Institute of Technology
Wasylenki LE, Baker MB, Kent AJR, Stolper EM (2003) Near-solidus melting of the shallow upper mantle: partial melting experiments on depleted peridotite. J Petrol 44:1163–1191
Webster JD, De Vivo B (2002) Experimental and modeled solubilities of chlorine in aluminosilicate melts, consequences of magma evolution, and implications for exsolution of hydrous chloride melt at Mt. Somma-Vesuvius. Am Mineral 87:1046–1061
Webster JD, McBirney AR (2001) The dramatic effect of chlorine on magmatic phase relations. Eos Trans Am Geophys Union 82:F1358